USING STEADY STATE AND TIME RESOLVED RAMAN SPECTROSCOPY TO STUDY THE MOLECULAR MECHANISM OF VOLUME PHASE TRANSITION OF POLY(N-ISOPROPYLACRYLAMIDE)

by

Tsung-Yu Wu

Bachelor of Science, James Madison University, 2014

Submitted to the Graduate Faculty of

The Kenneth P. Dietrich School of Arts and Science in partial fulfillment

of the requirements for the degree of

Master of Science

University of Pittsburgh

2017

UNIVERSITY OF PITTSBURGH

DIETRICH SCHOOL OF ARTS AND SCIENCES

This thesis was presented

by

Tsung-Yu Wu

It was defended on

December 15th, 2016

and approved by

Sean Garrett-Roe, Assistant Professor, Department of Chemistry

David Waldeck, Associate Professor, Department of Chemistry

Thesis Director: Sandy Asher, Distinguished Professor, Department of Chemistry

USING STEADY STATE AND TIME RESOLVED RAMAN SPECTROSCOPY TO STUDY THE VOLUME PHASE TRANSITION MOLECULAR MECHANISM OF POLY(N-ISOPROPYLACRYLAMIDE)

Tsung-Yu Wu, MS

University of Pittsburgh, 2017

Thermo-responsive hydrogels undergo volume phase transition (VPT). The temperature responsive VPT can be utilized for preparation of 'smart' materials. An ideal smart responsive material (SRM) would be triggered by a slight chemical or environmental change and respond in a desirable and reproducible way. Cross-linked Poly(N-isopropyl)acrylamide (PNIPAM) has one of the largest and fastest VPT, exhibiting a volume difference up to 30 fold within 1 μs when temperature increases past the lower critical solution temperature (LCST). As a result, PNIPAM is a great candidate for developing SRM. However, even though PNIPAM is the most widely studied thermal responsive polymer, a deep understanding of the molecular mechanisms involved in the VPT is still lacking.

Our previous study found the time constant for dehydration of the amide group (B) during VPT to be ~360 ns. In this study, a visible temperature jump (T-jump) Raman instrument was constructed to monitor the vibrational frequency of the isopropyl group (A) and methylene backbone (C) that PNIPAM undergoes during VPT, as seen below. We found the VPT molecular mechanism occurs as the following: As the temperature elevates, the dehydration of the isopropyl groups occurs very quickly with a time constant ~68 ns; shortly after, the dehydration of the polymer chains occurs with a time constant ~104 ns. Finally, the dehydration of the amide group occurs with a time constant ~ 360 ns.

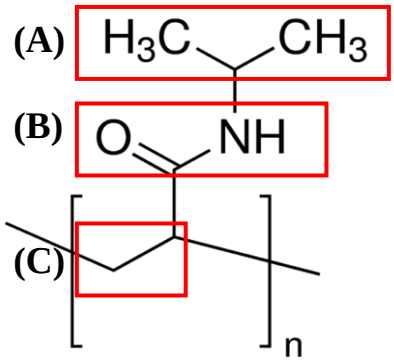

TABLE OF CONTENTS

LIST OF TABLES

LIST OF FIGURES

1.0 IMPORTANCE OF UNDERSTANDING VOLUME PHASE TRANSITION IN POLY(N-ISOPROPYLACRYLAMIDE)

Poly (N-isopropylacrylamide) (PNIPAM) thermally responsive polymer was first synthesized in 1956. Since then, it has become the most widely studied temperature responsive hydrogel. Light scattering technique, differential scanning calorimetry (DSC)[1-2], fluorescence spectroscopy[3-5], viscometry[6], NMR[7], and vibrational spectroscopy[3, 8-14] have been used to study the responsive behavior of PNIPAM. Theoretical and computational methods have also become a popular technique utilized to further understand this phenomenon.[15] Furthermore, PNIPAM is used in many applications over the years, such as drug delivery[16-18], artificial muscles[19], chemical sensors[20-22], microvalves[23-24], and smart materials[25-26]. Despite the large number of studies on PNIPAM, little is known about the molecular mechanism of its VPT. A more detailed understanding of VPT will aid the development of more precise and controllable smart materials. Our time resolved Raman spectroscopy studies will be able to monitor PNIPAM's VPT in a molecular level, and physically obtain a reaction coordinate of its VPT.

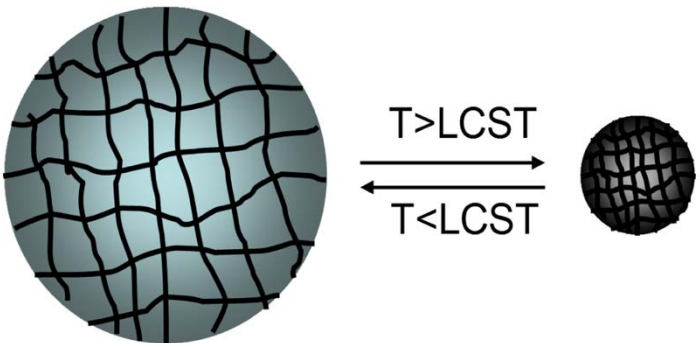

Figure 1. Volume phase transition (VPT) of cross-linked PNIPAM hydrogel. Below LCST, hydrogel is in a hydrated state. Above LCST, the hydrogel is in a compact and dehydrated state.

Linear chain PNIPAM undergoes a reversible, discontinuous coil-to-globule transition as temperature increases to above the lower critical solution temperature (LCST). The coil-to-globule transition in PNIPAM is analogous to the cold denaturation of globule proteins.[27] Above LCST, linear PNIPAM chains are in a globular folded state, and unfold to an extended state as it is cooled below LCST. A loosely cross-linked PNIPAM hydrogel, on the other hand, exists in a swollen hydrated configuration below its LCST. In the swollen state, PNIPAM's refractive index is nearly the same as water, making the hydrogel optically transparent in aqueous solution. As temperature increases above the LCST, the polymer undergoes a discontinuous volume phase transition (VPT) where water is quickly expelled from the PNIPAM hydrogel network and becomes compact and dehydrated state with a refractive index greater than that of water (Figure 1). The refractive index of the PNIPAM hydrogel increases. The VPT of PNIPAM is the largest and fastest of all known thermally responsive polymers, exceeding up to 30-fold volume change in 1μs.

Here we used dynamic light scattering, steady state-, and time resolved Raman spectroscopy to study the VPT of PNIPAM. A nanosecond visible Raman temperature jump (T-jump) apparatus was constructed to collect time-resolved measurements to investigate the VPT of PNIPAM. We determined the molecular mechanism by monitoring the frequency of multiple local vibrations at short timescales (10 - 5000 ns) after VPT is induced. This allows us to elucidate the

order of events involved in the VPT. These nanosecond timescale kinetic Raman data will allow us to time resolve the VPT and detect any intermediate spectral changes during VPT that steady state Raman data cannot provide. We found as the temperature elevates past LCST, the dehydration events occur in the following sequences: isopropyl group (~68 ns), methylene main chain (~104 ns), and amide group (~360 ns).

1.1 BACKGROUND ON VOLUME PHASE TRANSITION OF PNIPAM

The current VPT understanding mainly derives from the polymer Flory-Rehner theory that relate VPT to the contacts of polymer with solvent.[28] VPT is caused by an osmotic swelling pressure generated by changes in the free energy of mixing, the elastic free energy associated with crosslink constraints, and electrostatic interactions.[29] In terms of osmotic swelling pressure, this can be written as:

$$\Pi_{mix} + \Pi_{elastic} + \Pi_{elec} = 0$$

Π_{elec} is the electrostatic interactions of charges on the polymer chains. However, since PNIPAM is a nonionic polymer, this term will not be discussed.

The thermodynamic equation for the free energy of mixing between polymer and solvent is defined as a balance between entropic effects and enthalpic effects, $\Delta G_m = \Delta H_m - T\Delta S_m$. The free energy of mixing (ΔG_m) measures how well the polymer and solvent mix together. The entropy of mixing (ΔS_m) derived from the ordered water molecules in the vicinity of the polymer. The enthalpic contribution to mixing (ΔH_m) is from solvation of the polymer, as well as the balance between intra- and intermolecular forces.[30]

Entropy is a critical contributor to LCST behavior. Studies show that water molecules tend to arrange themselves into a "cage like" structure around the hydrophobic group to minimize contacts since they cannot hydrogen bond.[31-32] This results in a large decrease of entropy upon mixing (negative ΔS_m) because the water molecules exhibit preferential orientation. However, at low temperature the exothermic enthalpy contributed by the hydrophilic groups stabilizes this large entropy penalty coming from the hydrophobic groups. As temperature increases past the LCST, $\Delta G_m > 0$, the entropy of the system dominates forcing water out of PNIPAM network. PNIPAM then becomes a compact dehydrated state (Figure 1).

The elastic volume crosslink constraints ($\Pi_{elastic}$) is governed by the elastic restraining forces of the cross-linked polymer chains. It is a limiting factor on the extent of swelling. These elastic restraining forces are entropic in nature because stretching of the polymer matrix reduces the number of available chain conformations.[30, 33]

The VPT of PNIPAM is derived from changes in the free energy of mixing. The elastic free energy does not change because it requires a large amount of energy to break the covalent cross-links between PNIPAM chains in the hydrogel. Stimuli that affect the balance between entropy and enthalpy of mixing can trigger the VPT of PNIPAM, for example, a change of temperature, pressure, pH, or solvent properties[3, 27]…etc. Although there are multiple competing theories to explain the fundamental phenomena of the PNIPAM VPT, there is still no consensus about the molecular mechanism(s) driving the VPT.

1.2 PREVIOUS STUDIES ON VOLUME PHASE TRANSITION OF PNIPAM

Since 1956, groups have extensively studied the thermodynamics of VPT of PNIPAM using various methods with the goal of developing a deep understanding of the phenomenon. Vibrational spectroscopy has the unique ability to study conformational changes and local interactions of molecules. Thus, this technique can be used to study the hydration of PNIPAM. Amide vibrations, OH stretching bands, and the C-H stretching bands were often used to get insights into VPT in PNIPAM. Ramon *et al.* and Katsumoto *et al.* both use FTIR with attenuated total reflectance (ATR) to study the coil to globule transition of PNIPAM.[11] Ramon *et al.* deconvoluted the AmI, AmII, and water O-H stretching bands and analyzed the hydrogen bonding changes during the phase transition. They concluded that the phase transition consisted of two steps: the breaking of intermolecular hydrogen bonds between the amide groups of the polymer and the solvent initiates the phase transition. Consequently, an increase in intramolecular hydrogen bonding between –N-H and –C=O, which induced a coil–globule transition.[11] Subsequently, Katsimoto *et al.* observed frequency downshift of AmI band as water hydrogen bonds to the C=O group, and a frequency upshift as a water intermolecular hydrogen bond forms between water and the –N-H group. Their DFT calculation concluded that AmIII band is very sensitive to the conformational change of the molecule.[9]

Some studies on the other hand suggested that the property of water is a key factor in the phase transition of PNIPAM. Maeda *et al.* studied the hydration of the linear PNIPAM chain using FTIR spectroscopy, and found that the structure and properties of the water play a key role in determining the LCST of PNIPAM. Terada *et al.* studied the structure of water around PNIPAM (interfacial water) via Raman spectroscopy. They proposed that bulk water and interfacial water have different spectral characteristics.[34] Suzuki *et al.* studied the low frequency of water vibrations

in PNIPAM hydrogel via Raman spectroscopy and concluded that gel collapse is induced by destruction of the tetrahedral structure of water.[35]

Ahmed *et al.* further investigated the mechanism of VPT of PNIPAM using dynamic light scattering and time resolved UV Resonance Raman spectroscopy (UVRR). They found that one of the two hydrogen bonds between water and –C=O group is lost and they believed the hydrogen bonds of the water−amide (−NH) group remain unperturbed even in the compact dehydrated state above the critical temperature. They concluded that both polymer-water and polymer-polymer interactions play a key role in determining the VPT and the LCST of PNIPAM.[36]

A molecular mechanism of PNIPAM was proposed by two authors using two-dimensional correlational spectroscopy (2D-COS). Both Sun *et al.* and Lai *et al.* studied PNIPAM in D_2O using a combination of FTIR and 2D-COS to propose a mechanism of its phase transition.[10, 12] However, their conclusions are very different. Lai *et al.* found that the less hydrated methyl groups went through a rapid change between 29.1°C to 33.1°C. They suggested the dehydration of methyl groups is a three-step process. In addition, they proposed that as the temperature increases, amide groups in the side chains firstly break hydrogen bonds with water, and form intramolecular hydrogen bonds between the –NH groups and C=O groups so that polymer chains start to aggregate together. Then methyl groups in side chains dehydrate and finally the $–CH_2$ in main chain dehydrates. Sun *et al.*[10] also uses FTIR/ 2D-COS method to understand the hydrophobic collapse of PNIPAM hydrogel. They proposed a three-step dehydration process. Their proposed mechanism suggested the dehydration of isopropyl methyl groups occurs first, followed by aggregation of the main chain. Then, the breakage of the hydrogen bonds with the amide groups (–N-H) occurs, followed by the breakage of the hydrogen bonds with C=O groups. Ultimately, the hydrogen bonds form between C=O and N-H groups. Another 2D-COS study of PNIPAM hydrogel's VPT done

by Sun *et al.* suggested that as temperature increased to above LCST, PNIPAM hydrogel collapsed along the backbone before water molecules were expelled from the polymer network.[13] They concluded that this process was driven by the conversion of water-amide intermolecular hydrogen bonds to intramolecular hydrogen bonds.

As discussed above, a variety of molecular mechanisms of VPT have been proposed. Our time resolved Raman spectroscopy method can confirm the correct mechanism of VPT by physically timing the order of reaction. We hypothesized the VPT of PNIPAM occurs in three steps. Firstly, the dehydration of isopropyl groups (Figure 2A), followed by a structural rearrangement of PNIPAM. Secondly, the dehydration of Amide groups (Figure 2B). Finally, the dehydration and aggregation of the polymer main chains (Figure 2C). As much as the PNIPAM phase transition has been studied, there is still not a consensus for the mechanism of VPT of PNIPAM. Details of the dehydration dynamic processes will advance us toward the development of smart applications.

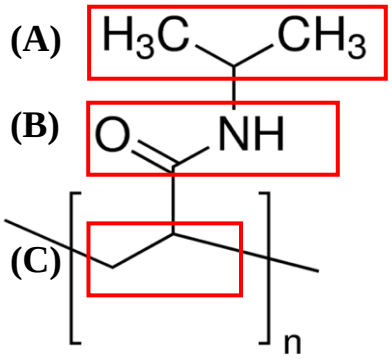

Figure 2. Molecular structure of PNIPAM contains (A) isopropyl group, (B) amide group, and (C) methylene polymer chain

2.0 RAMAN SCATTERING

Similar to IR spectroscopy, Raman spectroscopy is one of the fundamental types of spectroscopy used to identify the molecular structure and properties. Raman spectroscopy utilizes the fact that each molecule has a different set of vibrational energy levels, such that the photons emitted off the molecule have unique wavelength shifts. Each wavelength shifts in the spectra corresponds to specific vibrational modes and is unique to each molecular structure examined. [37-38]

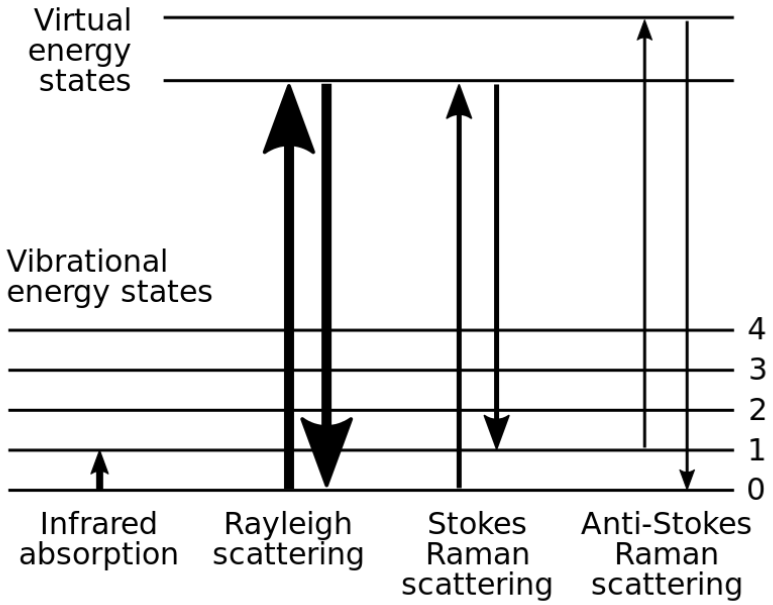

Figure 3. Energy diagram of IR absorption, Rayleigh scattering, Raman stokes scattering, and Raman anti-stokes scattering

When light interacts with matter, it can be either absorbed or scattered. As seen in Figure 3, the energy of the incident photon in infrared absorption spectroscopy is absorbed by a molecule which then causes the amplitude of the particular vibration to change. Since every bond has different energies, the incident photon therefore needs to correspond to the energy gap between the ground state and the excited state of a molecule.[38] However, in the case of scattering, any

wavelength of light can be used to get scattering from molecules.[37] The scattering process can be explained using classical theory as following: the scattering occurs when an electromagnetic wave (ex: incident light) interacts with the molecule, the electron cloud of the molecule is perturbed by the oscillating frequency of the electromagnetic wave. Therefore, creates an induced dipole moment within the molecule. As long as the electric field of the incident wave is not too strong, the induced dipole moment should be linearly proportional to the electric field, which is determined by:

$$P_{ind} = \alpha E \tag{1}$$

where the α is the polarizability of the molecule and E is the strength of electric field of the incident light.[39] This induced dipole moment will then radiate energy in a form of scattered light. The majority of the light is elastically scattered with the same frequency as the incident light $v_s = v_I$, which is referred to as Rayleigh scattering. On the other hand, small amount of light is inelastically scattered with frequency that is shifted from the incident frequency, $v_s = v_{I \pm} v_r$. This process is called Raman scattering, this occurs due to the interchange of energy between the photon and molecule. In addition, only the vibrations that have a change in polarizabiliy of the molecule will produce Raman scattering. The classical theory of the Raman effect explains it as: when the incident electromagnetic wave interacts with the molecule, the molecule will be perturbed by oscillating electric field and the time dependent dipole moment of the molecule will look like:

$$P = \alpha E_o \cos(2\pi v_o t) \tag{2}$$

As mentioned earlier, the polarizability α is a tensor that measure of how easy it is to polarize the molecule along each direction. It is a characteristic of a molecule that depends on its molecular structure and bond strengths. The polarizability can be expressed using Taylor series in the normal coordinates of the molecule:

$$\alpha(Q_k) = \alpha_o + \sum_k (\frac{\partial \alpha}{\partial Q_k}) Q_k + \cdots \quad (3)$$

Where α_0 is the polarizability at the equilibrium, and Q_k is the coordinate of the k^{th} normal mode relating to the vibration mode with frequency v_k. The vibrational normal coordinate Q_k will also oscillate in time:

$$Q_k = Q_{ko} \cos(2\pi v_k t) \quad (4)$$

Combining equation (2), (3), and (4) into equation (1) then the resulting equation for the induced dipole will be:

$$p = \alpha_o E_o \cos(2\pi v_o t) + \sum_k \left(\frac{\partial \alpha}{\partial Q_k}\right) Q_k E_o \cos(2\pi v_k t) \cos(2\pi v_o t) \quad (5)$$

Using a trigonometry identity, we can further convert equation (5) to[37, 39-40]:

$$p = \alpha_o E_o \cos(2\pi v_o t) +$$

$$\sum_k \left(\frac{\partial \alpha}{\partial Q_k}\right) \frac{Q_k E_o}{2} [\cos\{2\pi(v_o - v_k)t\} + \cos\{2\pi(v_o + v_k)t\}] \quad (6)$$

Equation (6) demonstrates the classical theory of the induced dipole moment. It shows there are clearly three terms, the first term describes the elastic scattering (Rayleigh scattering), the second terms describe the frequency shifted scattering (Raman scattering). As equation (6) illustrates, there are two types of inelastic scattering: Raman Stokes scattering which describes a downshifted frequency and Raman anti-Stokes scattering which is referred to as upshifted frequency. An important term worth mentioning is $\frac{\partial \alpha}{\partial Q_k}$ in the second term, which describes the change of polarizability in respect to normal coordinate. In order for Raman scattering to occur, this term has to be non-zero. In the case of a molecular vibration without a change of polarizability, Raman scattering will therefore not occur.

Raman spectroscopy has significant advantages over many analytical techniques. Some important advantages include non-destruction of the sample via light scattering, high selectivity,

high sensitivity, and very importantly, minimal sample preparation. In general, Raman spectroscopy is a powerful tool for identification of materials. However, Raman scattering is a relatively weak process, the number of Raman scattered photons are quite small. Later on, people found different ways to enhance the Raman intensity signal, which is referred to resonance Raman spectroscopy (RR).

2.1 RESONANCE RAMAN SPECTROSCOPY

Although classical theory provides a good level of understanding to treat Raman scattering, it cannot predict the molecular origin of Raman scattering. Resonance Raman scattering will be best described using time-dependent perturbation theory. The energy of the incident light in normal Raman scattering is much lower than the electronic transition of the molecule. Resonance Raman scattering on the other hand occurs when the energy of the excitation is within the electronic absorption of the molecule. As the incident light interacts with the molecule, the molecule is excited to a virtual state which immediately undergoes emission from the virtual state back to the frequency shifted final ground state. The Raman polarizability tensor is best described with equation (7).

$$(\alpha_{\rho\sigma})_{fi} = \frac{2\pi}{h}\sum_{r\neq i,f}\left\{\frac{\langle f|\hat{p}_\rho|r\rangle\langle r|\hat{p}_\sigma|i\rangle}{\omega_{ri}-\omega_o-i\Gamma_r} + \frac{\langle f|\hat{p}_\sigma|r\rangle\langle r|\hat{p}_\rho|i\rangle}{\omega_{rf}+\omega_o-i\Gamma_r}\right\} \quad (7)$$

Equation (7) is the KHD expression illustrates the polarizability tensor of the molecule excited by an electromagnetic (EM) wave as sums over the vibronic states of the molecule.

The subscripts are the normal coordinates of different states. $\sum$ indicates the sum over all vibronic states of the molecule, and the subscripts *r*, *i*, *f* denotes to excited vibronic state, initial

vibronic state, and final vibronic state respectively. The numerators are the transition electric dipole integrals describing the simultaneous mixing of the vibronic states in Raman scattering. ω_{ri} and ω_{rf} in the denominator are the frequencies of molecular oscillation at different transitions. ω_o is the frequency of incident light. Γr is the damping constant at the excited state which arises from the lifetime of the intermediate state. In Resonance Raman scattering, the denominator of the first term becomes negligible because the frequency of the incident light approaches the frequency of the excited electronic state. Therefore, for the Resonance condition, the KHD expression will be dominated by the first term. This term is referred to as the resonance term. The second term is called the non-resonance term. ω_{rf} and ω_o are added together in the denominator, the second term will always be large compared to that in the first term. Consequently, the second term plays a smaller role in describing the polarization process and will now be neglected.[38] The KHD expression suggests that as the excitation wavelength of the incident light approaches the electronic transition of the molecule, the amplitude of the oscillation will be larger. Therefore, the vibrations will be enhanced as the induced dipole moment increases.

UV resonance Raman spectroscopy (UVRR) particularly has become more widely used because of several advantages. For example, UV Raman has significantly less fluorescence interference compared to visible Raman. Another main advantage is that many compounds absorb in the UV. By changing the excitation wavelength in the ~200nm region, we can selectively tune into the $\pi \rightarrow \pi^*$ electronic transition of the amide bonds to get enhancement on different bands. This enhancement can be up to a factor of 10^8.[38, 41-43] Numerous studies utilized this selective enhancement of UVRR to monitor hydrogen bonding and solvent exposure of proteins and polymers which contain amide groups.[36, 44-46]

3.0 INVESTIGATING ON PNIPAM C-H STRETCHING BANDS OF STEADY STATE VPT USING RAMAN SPECTROSCOPY

Up to this day, thermodynamics has shown the hydrophobic isopropyl moiety plays a major role in VPT of PNIPAM. Although some other studies suggested the dehydration of the hydrophilic group is the initial driving force to VPT.[10, 13] Most spectroscopic research studies on the VPT of PNIPAM have been mainly focusing on the Amide vibrations.[3, 9-11, 13, 36, 46-47] The vibrations of the hydrophobic isopropyl groups have not been studied much in detail. Most research studies reported only the observation of the CH stretching bands down shifts in frequency, as the temperature increases across LCST.[3, 9-10, 12-13, 15, 47-48] Evidence has shown that the C-H stretching vibration is sensitive to the environment and solvation, especially the CH_3 anti-symmetric stretching mode of PNIPAM.[4, 10-13, 46, 49-52] The greater the number of solvating waters around a methyl group, the higher the frequency of the C-H stretching vibration. This has been explained by different theories, including blue shifting hydrogen bonding and conformational changes of the methyl groups.[53-57] A shift toward higher frequency of the C-H stretching bands upon hydrogen bonding indicates a strengthening of the C-H...O hydrogen bond. In other words, a contraction of the C-H bond length. This behavior is opposite to the classical hydrogen bond, and the mechanism of it is not well understood.

The study of water vibration bands can give an atomistic picture of the local structures of water and their structural evolution with respect to temperature and time. Understanding the water dynamics around the polymer (interfacial water) is the key to explain fundamental physical phenomena such as the polymer phase transition. However, this is very challenging mainly because it is difficult to selectively probe the dynamic response only from the interfacial water. As a result,

most of our current understanding derived from theoretical studies.[49, 58-60] On the other hand, time resolved Raman spectra of PNIPAM VPT can provide useful insights about the path of the interfacial water molecules. Moreover, the band assignments at the CH stretching region is still extremely vague due to the complexity of overlapped CH bands from –CH group, -CH_2 group, and -CH_3 group. Using Raman spectroscopy, we will investigate the C-H stretching bands of steady state PNIPAM as it undergoes a volume phase transition.

3.1 EXPERIMENTAL SECTION

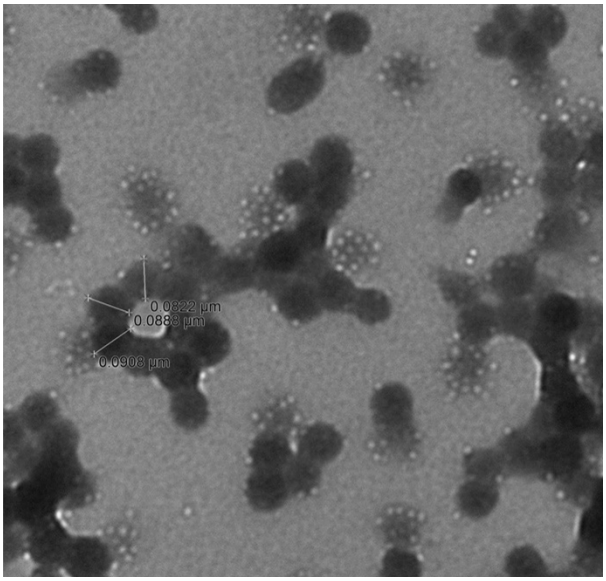

Figure 4. TEM image of PNIPAM nanoparticles in the collapse state

Sample preparation. PNIPAM nanoparticles were synthesized using the previously published technique.[61] The samples were synthesized using dispersion polymerization. 3.4730g of NIPAM, 0.0513 g of 2-acrylamido-2-methyl-1-propanesulfonic acid (ionic co-monomer, Aldrich), 0.1101 g of N,N′- methylenebisacrylamide (cross-linker, Fluka), 0.0815 g of sodium dodecyl sulfate (surfactant, Aldrich), and 0.0280 g of ammonium persulfate (initiator, Sigma-Aldrich) were added

to 250 mL of 18 MΩ deionized water and reacted at 70 °C for 4 hours under stirring. The product solution was filtered by glass wool and dialyzed against nano-pure water by using a Snakeskin dialysis tube for 4 weeks to remove unreacted monomers and impurities. Ionic impurities are removed by storing the PNIPAM particles with mixed bed ion exchange resins. The particle size was measured via Transmission Electron Microscope (TEM) (Figure 4) and dynamic light scattering. PNIPAM was concentrated by centrifuging the purified suspension at 17,000 rcf at 34°C for 70 minutes. The supernatant was removed and the final concentration was ~4 wt%.

Solid PNIPAM was prepared by drying concentrated PNIPAM particles on a gold-coated coverslip in a 70°C oven. Then, another layer of particles was deposited on top of the dried PNIPAM film and oven dried. This step was repeated four times to ensure a thick layer of sample when taking Raman spectra.

The deuterated samples of PNIPAM were prepared by immersing the PNIPAM particles into D_2O. Four tubes of 10 mL solution of 1.45 wt% PNIPAM in water was centrifuged at 17,000 rcf for 70 minutes at 29°C. The PNIPAM pellets were immediately removed. The PNIPAM particles were dried in the oven at 70ºC for three hours. They were re-dispersed into D_2O (99.9 atom % D, Cambridge Isotope Laboratories, Inc). The resulting concentration of PNIPAM in D_2O was ~0.10 wt%.

Dynamic light scattering. Sizes of the particles in aqueous state were measured using dynamic light scattering (Brookhaven, ZetaPALS) at different temperatures. The sample particles were diluted down to ~0.001 wt% for particle size measurement.

UVRR instrument. A home-built UV resonance Raman spectrometer was utilized which has been previously described.[62] A Coherent Infinity Nd:YAG laser produced 355-nm (third harmonic) 3-ns pulses at 100 Hz. 204 nm was generated by selecting the fifth anti-stokes line that

Raman-shifted of 355 nm using a 1-m tube filled with H_2. A Pellin Broca prism was used to select the 204-nm excitation. The liquid sample was circulated in a free surface, temperature controlled stream. The solid sample was attached to a spinning cell to avoid heating or accumulation of photochemical degradation products formed by the laser pulses. The Raman scattered light was imaged on a subtractive double spectrometer. The dispersed UV light was detected by CCD with a >30% quantum efficiency in the deep UV (Princeton Instruments Spec). A more detailed description is given by Bykov et al.[62]

Visible Raman Microscope (λ_{ex} = 633 nm). Renishaw inVia Micro-Raman Microscope was used with an excitation wavelength of 633 nm. The configuration was set to 1800 1/mm for grating with a 5x magnification objective.

Visible Raman instrument (λ_{ex} = 532 nm). The 532 nm visible Raman measurement were made using a Coherent Infinity Nd:YAG laser produced 3-ns pulses at 100 Hz. This beam was generated by frequency doubling from its fundamental wavelength (1064 nm). The visible Raman spectra of PNIPAM ~16 wt% were taken in a 10-mL vial using a 1200 G/mm grating. The visible Raman spectra of PNIPAM (~4 wt%) and diluted PNIPAM (~2 wt%) were taken using a 500 G/mm grating. The dispersed Raman scattered light was imaged onto a CCD detector (Pylon). PNIPAM (4 wt%) spectra were collected using a 1 cm cuvette placed in a temperature controlled cuvette holder. Precise temperature was directly measured using a Thermocouple. The diluted sample was circulated using a wire guided stream.[63] Detail description of the wire guided stream is given in Chapter 4.

3.2 RESULTS AND DISCUSSION

3.2.1 DLS Temperature Dependence Particle Size Measurements

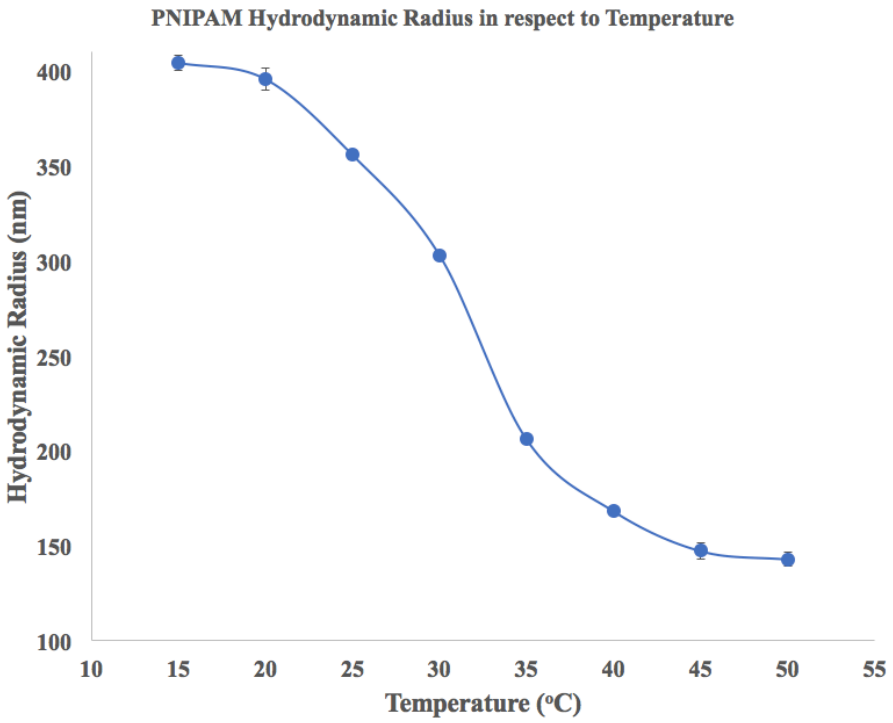

Figure 5. DLS measurements of PNIPAM hydrogel effective diameter as a function of temperature. The graph indicates a LCST~32ºC

PNIPAM nanogels (d= ~376 nm at room temperature) were synthesized as described in the experimental section. Figure 5 is the temperature dependent DLS measurements indicating a transition temperature of ~32ºC. As the temperature increases from 15 ºC to 50 ˚C, the particle size collapses from 404 nm to 143 nm with a total of 23-fold volume difference. Approximately, 6.22×10^8 water molecules are expelled out of the PNIPAM particles that contain ~2.8×10^6 monomers. This volume change suggests a ~95.6% reduction of water inside of PNIPAM hydrogel particles.

3.2.2 Steady State Raman Spectra of PNIPAM at Amide Region, λex = 204 nm

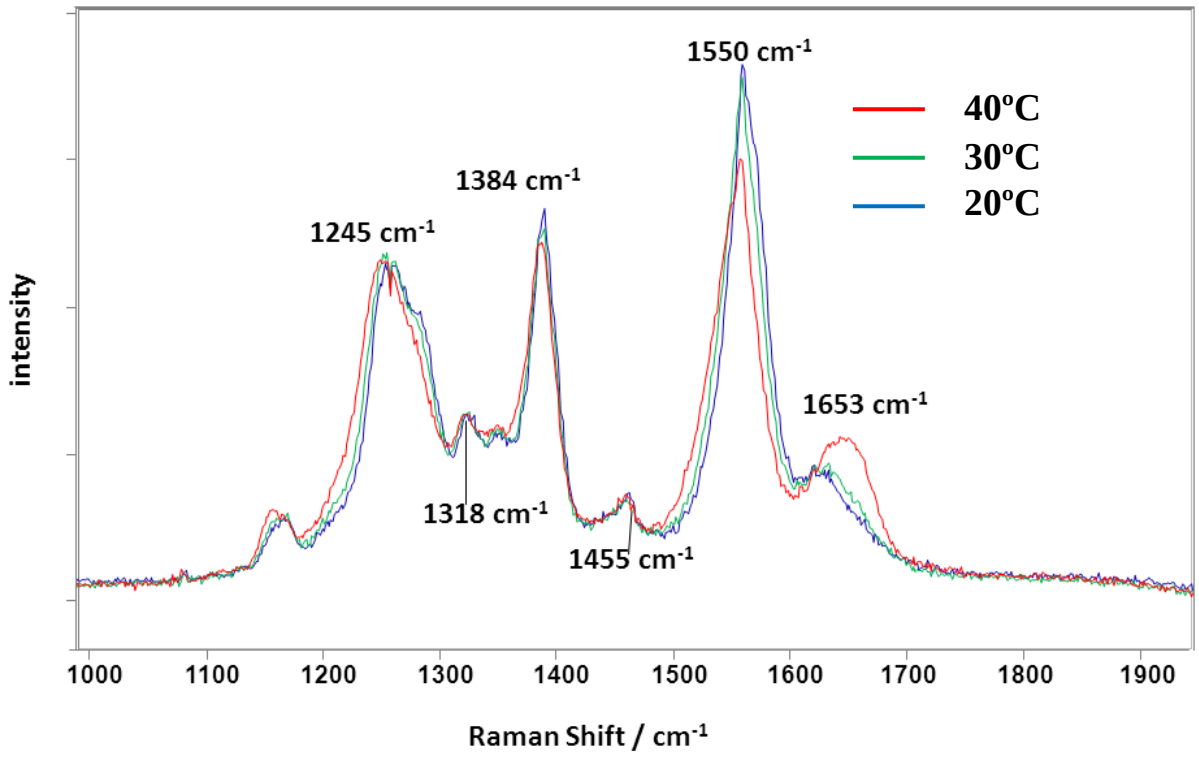

Figure 6. Amide region of UVRR (204 nm excitation) spectra of PNIPAM nanogel at 20ºC, 30ºC, and 40ºC.

Amide Region (1000-1700 cm^{-1})

The steady state UVRR spectra of the PNIPAM particles synthesized here were collected in the amide region as shown in Figure 6. Our results are consistent with the previous study done by Ahmed *et al.* and many others.[10, 12-13, 36, 51] The band at ~1653 cm^{-1} is the PNIPAM AmI band and it upshifts in frequency and increases in intensity as the temperature increases.[36] The AmI vibration is mainly derived from a C=O stretching motion, and the frequency is very sensitive to hydrogen bonding. The AmII (1550 cm^{-1}) vibration is mainly attributed to the C-N stretching and in phase N-H bending motions and it shows a slight downshift in frequency and large decrease in intensity as the temperature increases.

In contrast, the AmIII (1245 cm^{-1}) bands show slight downshift in frequency and no change in relative intensity as the temperature increases. The AmIII vibration arises mainly from the mix of C-N stretching and N-H in-phase bending motion.[36] The $C_\alpha H_\beta$ bending (1384 cm^{-1}) band also shows no significant change in frequency or intensity. [36, 64]

3.2.3 Steady State Raman Spectra of PNIPAM at CH Stretching Region, λex = 204 nm

CH stretching region (2850 – 3000 cm-1)

The steady state UVRR spectra of the C-H stretching region of the PNIPAM particles (~0.08 wt%) were collected at room temperature in both water hydrated state and dry solid state. Water was subtracted out of the UVRR spectra of the water hydrated PNIPAM, in order to see the C-H stretching bands (Figure 7). To our surprise, CH stretching bands at ~2950-3000 cm^{-1} cannot be found in the UVRR spectra. We assigned the observed bands as the amide overtone and combination bands. Since the Amide bands are selectively enhanced in the deep UV, the overtone and combination bands derived from the amide vibration are also enhanced. With bands assignment in the amide region, the observed bands at 2600 cm^{-1}-3300 cm^{-1} can be assigned as following. The bands at 2735, 3082, and 3288 cm^{-1} are assigned to the overtone of $C_\alpha H_\beta$ bending that is enhanced by coupling with N-H bending motion (1384*2=2768), AmII overtone (1550*2=3100), and AmI overtone (1653*2=3306), respectively (Table 1). The rest of the bands were assigned to combination bands (Table 2), where the band at 2626 cm^{-1} contains contributions of both AmIII and $C_\alpha H_\beta$ bending vibration (1245+1384=2629). The band at 2795 cm^{-1} was assigned to the combination band of AmI and AmII vibration (1653+1550=2795). The band at 2873 cm^{-1} was assigned to the combination band of AmII and AmIII vibration (1653+1245=2898), and the band at 3178 cm-1 was assigned to the combination band of AmI and AmII

(1653+1550=3203). The frequency of most of these observed overtone bands and combination bands are slightly less than the calculated vibration due to some anharmonicity. We concluded that the strong resonance enhanced amide overtone and combination bands makes it extremely challenging to observe C-H stretching vibrations with 204 nm excitation.

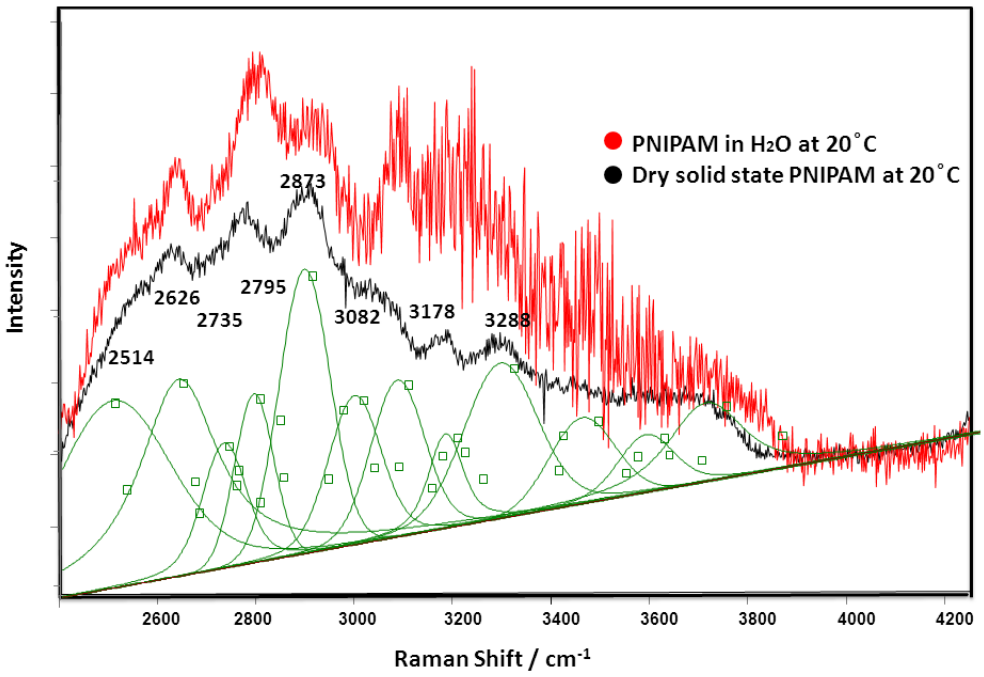

Figure 7. UVRR (204 nm excitation) spectra of CH stretching region of hydrated PNIPAM after water subtraction at 20ºC (red) and dehydrated solid state PNIPAM (black). Raman bands are fitted with Voigt profiles.

Table 1. Overtone bands assignment from the UVRR spectra of PNIPAM at the CH stretching region

Peak assignment	AmI overtone	AmII overtone	$C_\alpha H_\beta$ bending overtone
Peak estimation (cm^{-1})	1653*2=3306	1550*2=3100	1384*2=2768
Peak position (cm^{-1})	3288	3082	2735

Table 2. Combination bands assignment from UVRR spectra of PNIPAM at the CH stretching region

Peak Assignment	AmI+AmII	AmI+AmIII	AmI+AmII	AmIII+$C_\alpha H_\beta$ bending
Peak estimation (cm^{-1})	1653+1550=3203	1653+1245=2898	1653+1550=2795	1245+1384=2629
Peak position (cm^{-1})	3178	2873	2795	2626

To further confirm the PNIPAM bands observed in the CH stretching region on Figure 7 are either overtones or combination bands, UVRR spectra of PNIPAM in D_2O were collected (Figure 8). Upon deuteration, many peaks in the amide region will downshift, and intensities will change dramatically. The replacement of hydrogen at the amide group (-N-H) by deuterium will change the normal modes of the molecule. As a result, AmII and AmIII bands are affected significantly. According to the study done by Mayne and Hudson, the deuterated N-methylacetamide spectrum was dominated by the Amide II' vibration, which is mostly C-N stretching.[65] Since the strong AmII' peak is located at ~1475 cm^{-1}, quantitatively, we expect to see an AmII' overtone band at ~2900 cm^{-1} (1475*2=2950). To confirm this, the Raman spectral region from 2400 cm^{-1} to 3300 cm^{-1} was recorded of PNIPAM in D_2O at room temperature (Figure 8a). Table 3 illustrates the band assignments for PNIPAM in D_2O at the amide overtone region. The peak at 2920 cm^{-1} is the AmII' overtone band. The rest of the peaks at ~2463 cm^{-1}, ~2793 cm^{-1}, and 3080 cm^{-1} are assigned to combination bands. The band at ~2463 cm^{-1} is attributed to a combination of AmII' bending and the 1020 cm^{-1} band (1475+1020=2495). And the peak at ~2793

cm^{-1} is attributed to a combination of AmII' band and CH bending (1320+1475=2795). Lastly, the small peak at ~3080 cm^{-1} derived from a combination band of

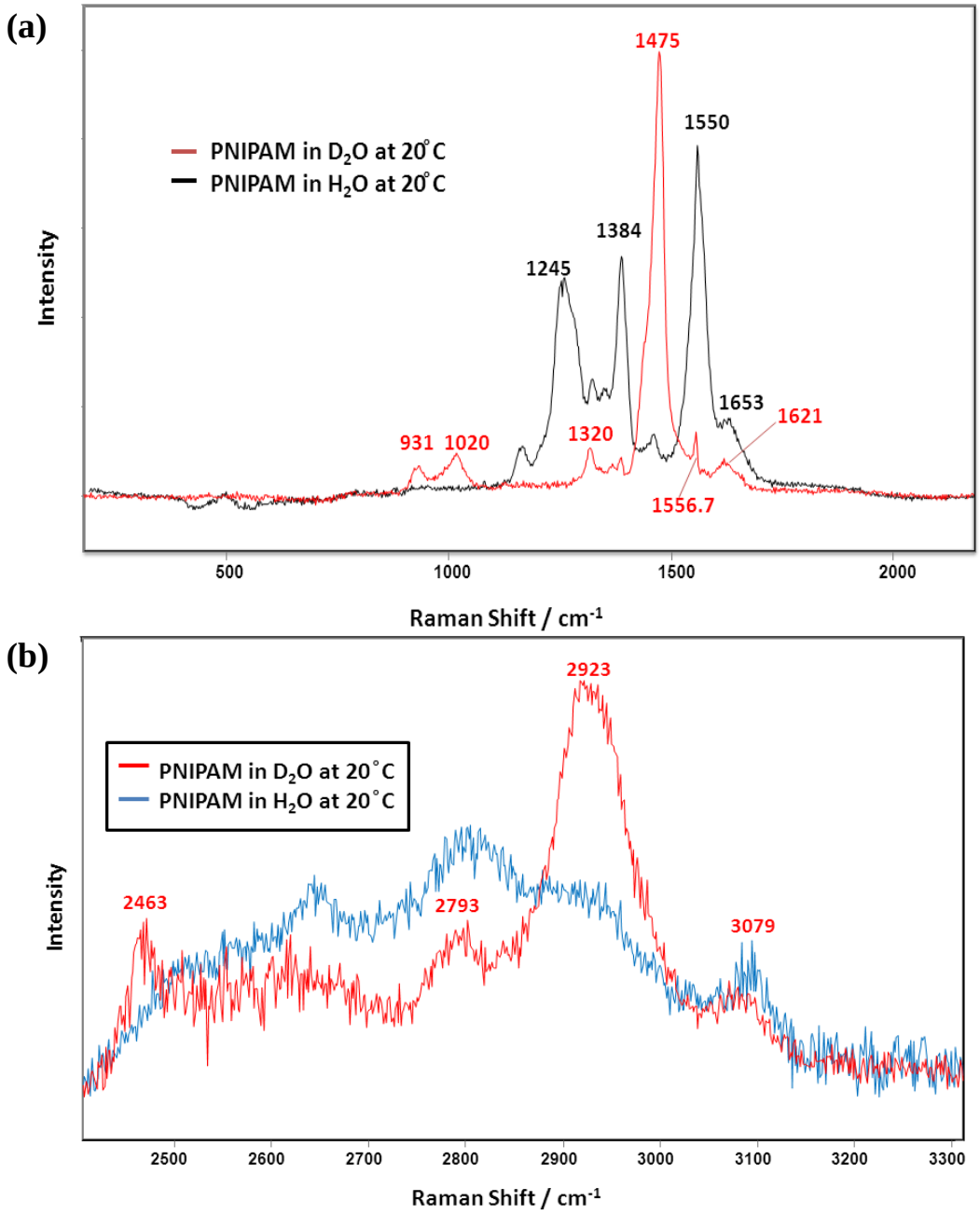

Figure 8. (a) 204-nm excitation UVRR spectrum of PNIPAM in D2O and H2O in the amide region (b) in the CH stretching region

AmI' and AmII' (1621+1475=3096). The spectra of PNIPAM in D_2O helped to further verify that the bands presented in Figure 7 are Amide overtone and combination bands (Figure 8).

Since we have concluded that the C-H stretching bands cannot be resolved at an excitation wavelength of 204 nm, due to the overlapping of the resonance enhanced amide overtones and combinations bands. Visible excitation must be used to see the C-H stretching bands.

3.2.4 Steady State Raman Spectra of PNIPAM at CH Stretching Region, λex = 532 nm

The YAG laser (1064nm) was used and frequency doubled to collect 532 nm excited PNIPAM spectra at the CH stretching region. The spectra of PNIPAM in aqueous state (~4wt%) of 18ºC, 43ºC, and solid state PNIPAM are shown in Figure 9. They were fitted with Voigt profile as five peaks (details in band assignments please refer to Appendix A).[66] The CH stretching peaks downshift in frequency as PNIPAM dehydrates from the fully hydrated form at 18ºC to dehydrated solid state. In particular, the CH_3 anti-symmetric band showed a ~7 cm^{-1} shift, and this is observed in previous studies as well.[51] The frequency changes can be related to the intermolecular interactions in PNIPAM such as hydrogen bonding. To understand the spectral changes of dehydration of the hydrophobic groups, it is best to correlate with the spectra changes in the water stretching vibrations. To do that, we need to increase wavelength coverage of the grating, which will decrease the spectral resolution.

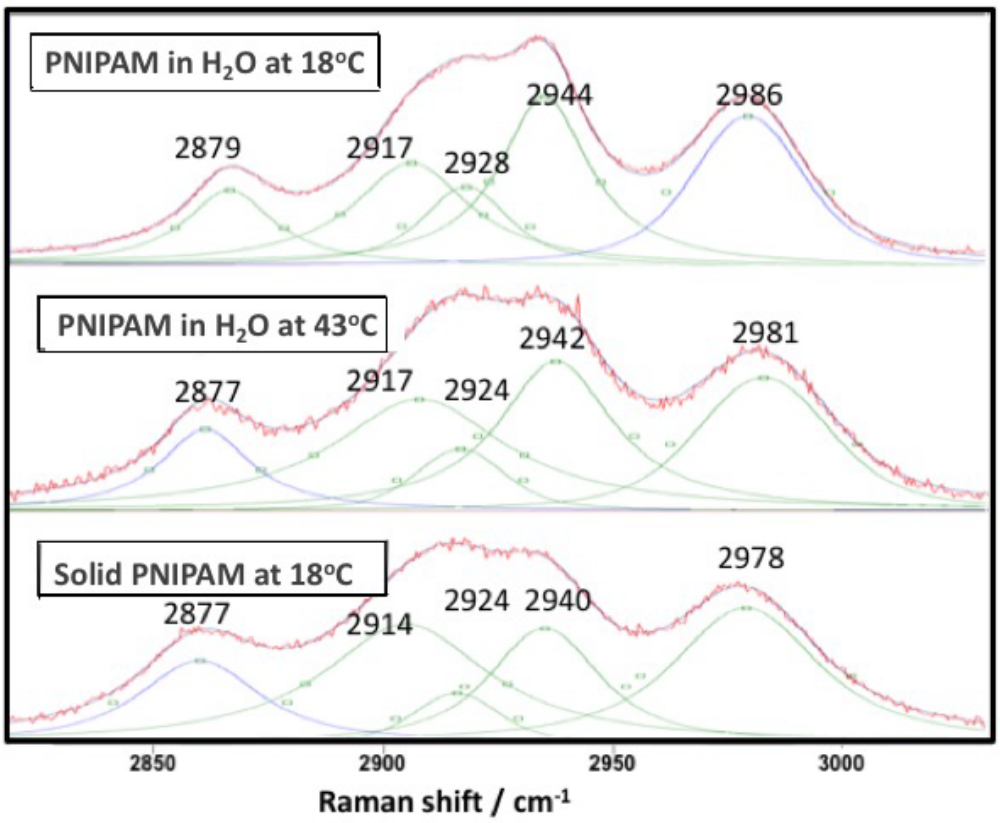

Figure 9. Visible Raman (532 nm excitation) spectra of CH stretching region of hydrated PNIPAM at 20°C, 43°C, and solid state PNIPAM at 20°C. Raman bands are fitted with Voigt profile. Please see 0 A for band assignments.

CH stretching and OH stretching region with 500G/mm grating (2800-3800cm^{-1})

Figure 10 shows the 532 nm excited Raman spectra of PNIPAM in H_2O (~4 wt%) using a 500 G/mm grating. The 500 G/mm grating allow us to monitor both the dehydration of the hydrophobic groups and the water stretching vibration without compromising too much spectral resolution. These spectra were further deconvoluted into three sub bands for the water stretching bands, and four bands for the CH stretching bands (Figure 10). The CH-2 band (Figure 10) at ~2925cm^{-1} arises from many bands such as two CH_3 Fermi resonance bands, CH stretching (trans), and CH_2 asymmetric stretching. These bands overlapped closely to each other so it is very hard to

resolve them. Therefore, in this case four bands are used to fit the CH stretching region. Please refer to Appendix A for details on CH stretching band assignments.

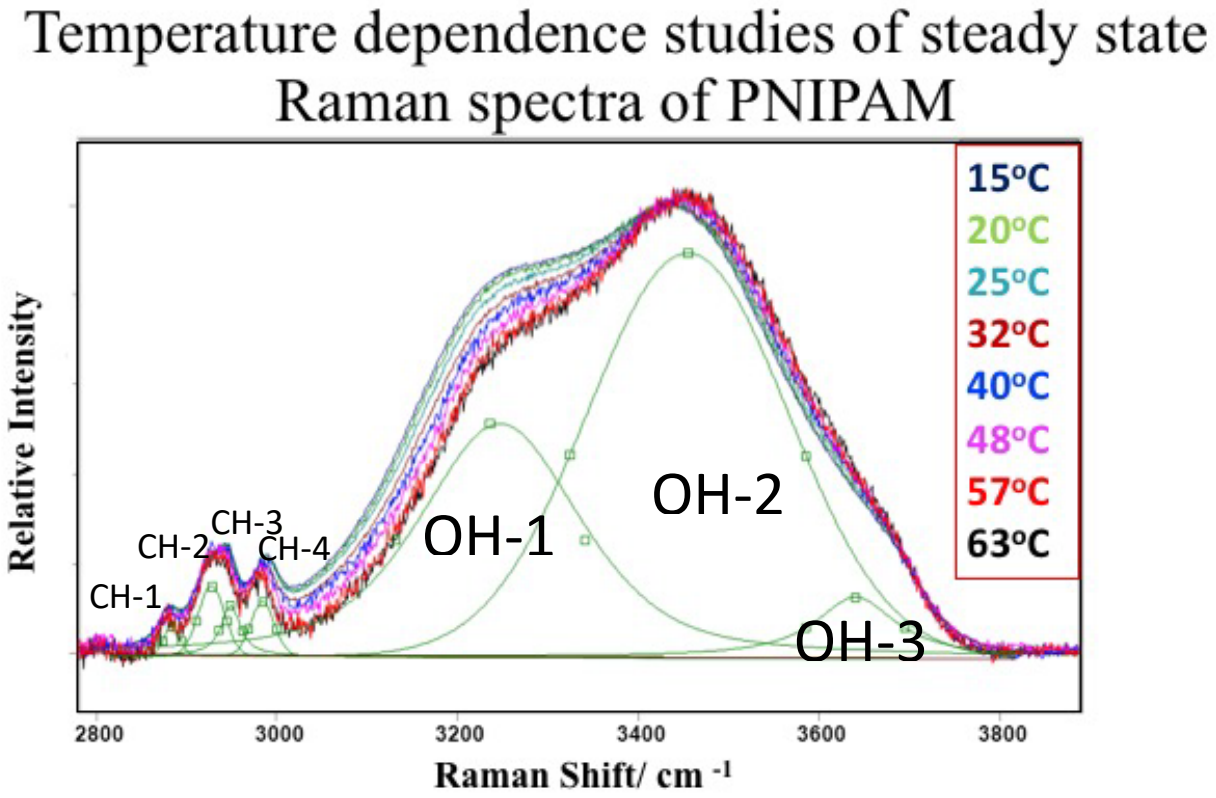

Figure 10. Visible Raman spectra (532 nm excitation) of PNIPAM in H_2O at indicated temperatures in both C-H stretching and O-H stretching regions. All bands are fitted with a minimum sum of mixed Gaussian and Lorentzian bands.

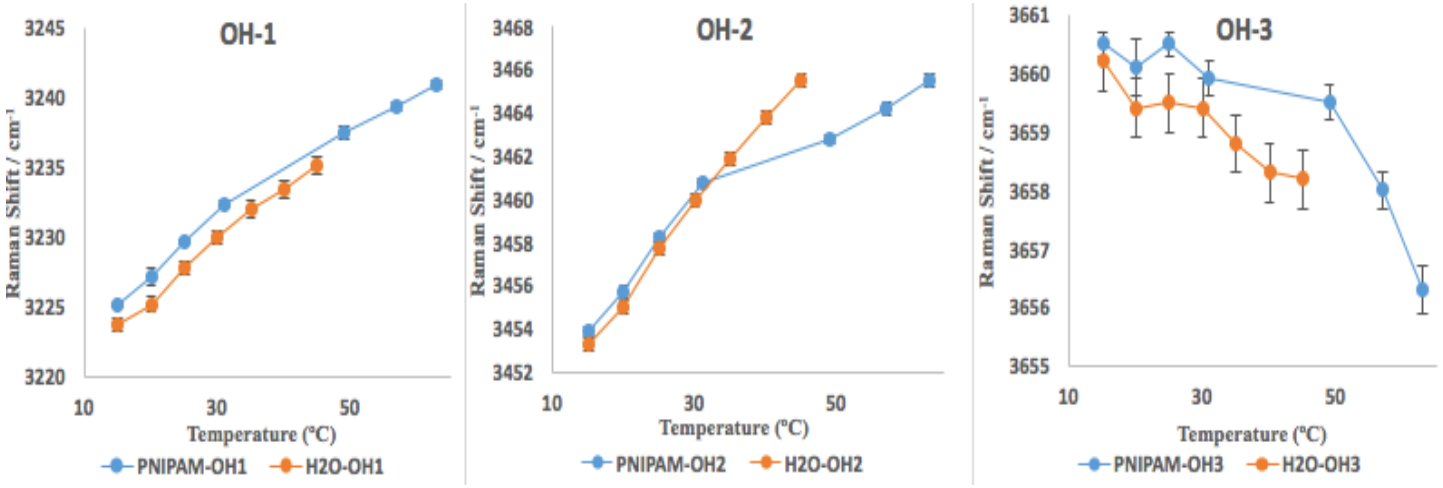

Figure 11. The frequency shifts of OH stretching bands as a function of temperature of PNIPAM in H_2O (blue) and pure water (orange)

Frequency shifts of the OH stretching bands from PNIPAM were plotted against pure water (Figure 11). The hydrogen bonding strength of water in PNIPAM is slightly weaker compared to the hydrogen bonding in pure water. The frequency shifts in respect to temperature between water OH stretching bands in PNIPAM and pure water is similar below LCST. However, as the temperature increases past LCST of PNIPAM, there is a decrease in frequency in OH-1 and a large downshift in frequency in OH-2. This suggests a stronger hydrogen bond between the water molecules. The changes of the hydrogen bonding strength after LCST may indicate a disruption of the tetrahedral hydrogen bonded bulk water. Suzuki *et al.* studied the low frequency Raman of PNIPAM gel and concluded as well that the disruption of tetrahedral hydrogen bonded water must play an essential role in the volume phase transition of PNIPAM gels.[35] Further low frequency Raman studies needs to be done to understand this.

As mentioned before, this result is consistent with the experimental work by Scatena *et al*. This suggests the attraction force between proximal water and PNIPAM become weaker as PNIPAM undergoes VPT.

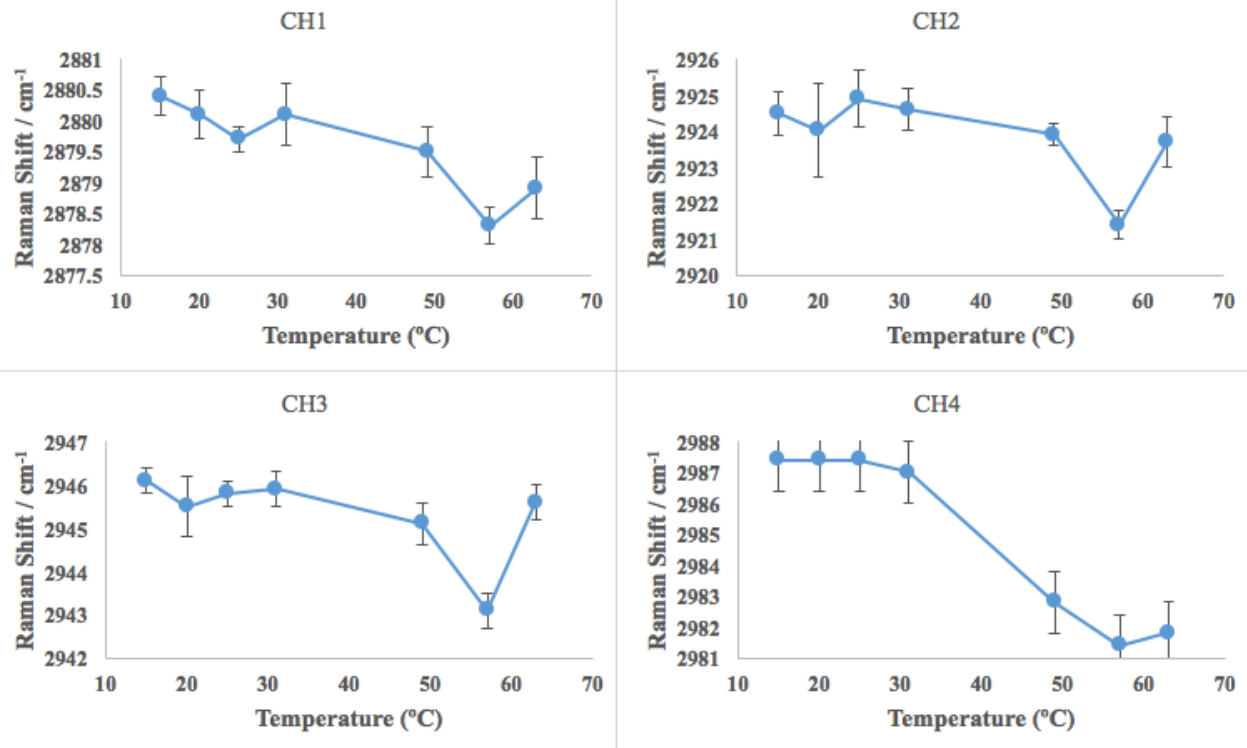

Figure 12. CH stretching bands frequency shifts in respect to temperature

As previous studies show, CH stretching bands undergoes frequency increase upon hydration, which is induced by the dehydration of the polymer.[8, 10, 12-13, 51] This observation is the opposite of the classic hydrogen bond. This phenomenon is referred to as blue shifting or improper hydrogen bonds. Most computational studies show the only difference between red shifting and blue shifting hydrogen bonding are the amplitudes of attractive or repulsive forces between the hydrogen donor and acceptor.[54-56, 67-70] The mechanism of the blue shifting is still not clear. However, we know the shift toward lower frequency in the CH stretching bands upon temperature increases past LCST indicate the dehydration of the isopropyl groups and the methylene main chain (Figure 12). The most down-shifted band is the CH_3 anti-symmetric stretching of PNIPAM (Figure 12). Although they all show an obvious downshifting as temperature increases to 35°C, the CH_3 anti-symmetric stretching band correlate most well with the hydrophobic collapse of PNIPAM (Figure 13). The CH str-1 and CH str-2 bands contribute from not only the methyl

groups, also from the CH group, and the methylene groups. Therefore, the CH_3 anti-symmetric stretching band is the best marker to monitor and determine the time constant for the dehydration kinetics of isopropyl groups.

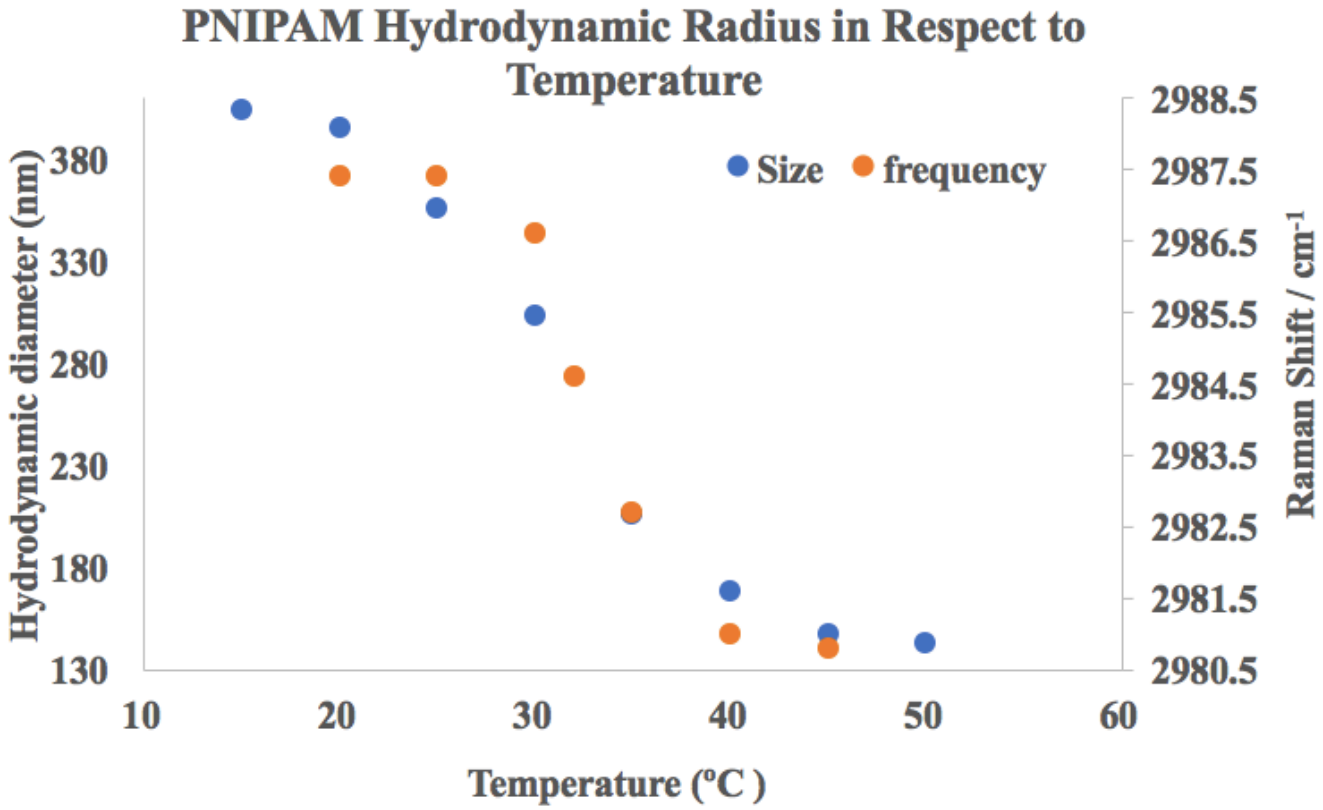

Figure 13. Frequency shift of CH_3 asymmetric stretching band of PNIPAM corresponds well with the change of particle size during VPT

3.3 SUMMARY

In UVRR studies of PNIPAM, we found the resonance enhanced amide overtone and combination bands mask the CH stretching bands of PNIPAM. Therefore, we used normal Raman to study the CH stretching bands at 532 nm. In the 532-nm excited Raman spectra of PNIPAM in water, the

OH stretching bands show a change in the hydrogen bonding between water molecules undergoing VPT. Most importantly, we observed a red shift of the CH stretching bands as the temperature increases. The CH_3 anti-symmetric stretching band show the largest red shift upon VPT, and we concluded this band is the marker to monitor the dehydration kinetics of the isopropyl groups.

4.0 CONSTRUCTING A NANOSECOND PUMP – PROBE TEMPERATURE JUMP SYSTEM TO STUDY THE KINETICS OF PNIPAM'S HYDROPHOBIC COLLAPSE

The process of the hydrophobic collapse of PNIPAM occurs extremely fast. According to Ahmed *et al*., the whole hydrophobic collapse occurs within 1 μs.[36] To study the mechanism of this collapse, we need a method that enable us to observe changes in a very short timescale. Scientists use different methods to collect kinetic measurements of reactions. The Nobel prize winning work, laser induced temperature jump (T-jump), is a powerful tool for studying the kinetics and mechanism of chemical reactions. [71-73] A laser induced temperature jump is a method that rapidly disturb the chemical equilibrium of a system through a change of temperature. By combining this technique with vibrational spectroscopy, one can obtain information on dynamics of protein folding in the ps – ns time scale.[44-45, 72, 74] The principle of the temperature jump method is described as the following: Typically, a time resolved temperature jump set-up utilizes two synchronized pulsed lasers. One laser acts as a heating laser ("pump"), the other one acts as a probing laser ("probe"). Essentially, the pump laser heats up the sample and very shortly after the probe laser induces Raman scattering that can be monitored to obtain chemical information at that particular moment. By monitoring the Raman signal as a function of the time delay (10 ns – 5 μs), we can obtain ultrafast information on any process initiated by the pump pulse.

Designing and building the Raman temperature jump set up, there are many things to be considered, such as resolution, wavelengths of lasers, gratings, space available…etc. To this date, there has not been a visible Raman temperature jump experiment successfully done because of the numerous challenges that come into play. In this chapter, experimental design and consideration of the 532-nm excited Raman temperature jump will be discussed.

4.1 EXPERIMENTAL METHODS

The scheme showed below is the 532-nm excited Raman T-jump set up that was constructed (Figure 14). The IR laser at 1.9 μm is chosen to be the heating pulse, and it directly heat up water in PNIPAM since water absorbs strongly at this wavelength. The 532-nm beam acts as a probing laser for probing the Raman response from the sample shortly after the IR heating beam. The heating pump beam is obtained by Raman shifting the YAG fundamental (1064 nm) in H_2 to 1.9 μm (first Stokes). And the probing beam at 532 nm was generated by frequency doubling from the fundamental Nd:YAG laser that emits photons at 1064 nm (Coherent infinity, Inc.). The 532-nm beam passed through a Pellin Broca prism. A dielectric mirror is used at 45º angle to reflect the 532-nm beam and transmit the 1.9 μm at 90º. Both beams are directed onto the sample by passing through two turning prisms. A focus lens (f=7.5 cm) is placed in between the two turning prisms to focus both beams onto the same sample overlaying volume. The Raman scatter light is collected and focused onto the slit of the spectrometer. Right before the slit, a Rayleigh rejected filter is used to prevent any Rayleigh scatter light from entering the spectrometer. The Raman scattered light is dispersed by a rule planed grating (Richardson Gratings) and sent to the CCD detector. By altering the delay time between the two lasers, we can obtain kinetic information on the nanosecond timescale.

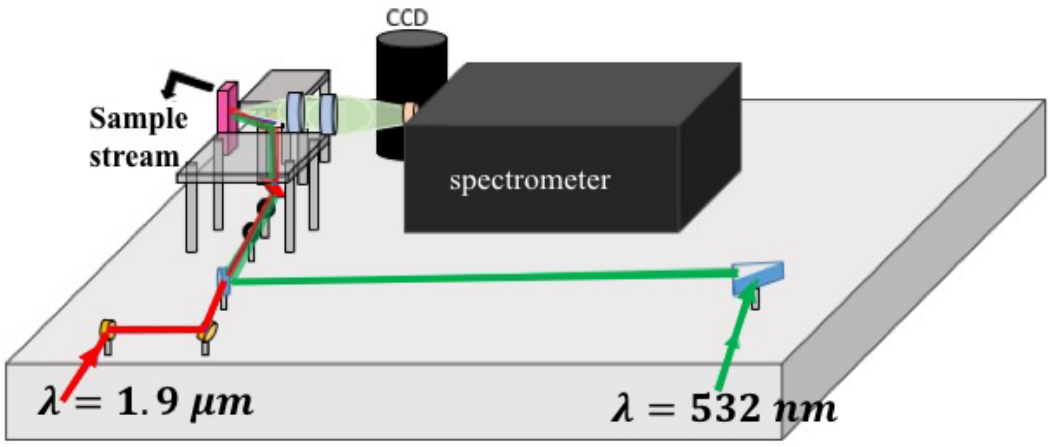

Figure 14. Schematic of visible Raman temperature jump set up. Green arrow indicates the path of the 532-nm visible laser. Red arrow shows the path of the IR heating laser.

4.2 EXPERIMENTAL CONSIDERATIONS

Grating. Choosing a grating is important because grating determines the spectral range and the spectral resolution of your spectrum. Our goal is to obtain kinetic information in both the water OH stretching region, and the CH stretching region. And the minimum wavelength coverage required is 1200 cm^{-1}. The groove density of the grating and wavelength coverage are inversely proportional to each other.

A rule planed grating with a groove density of 500 G/mm was purchased from Richardson Gratings. As expected, the wavelength coverage this 500 G/mm grating provided is ~1440 cm^{-1}.

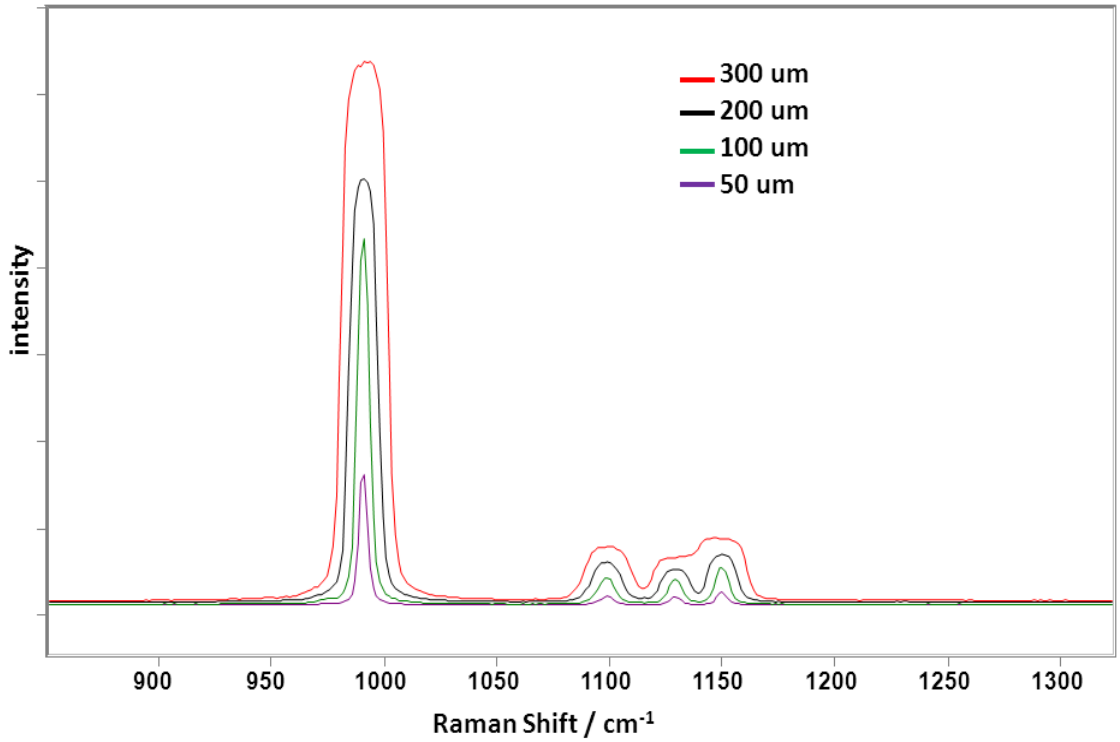

Figure 15. The effect of slit width on the band shape of solid Na_2SO_4.

Figure 15 shows the effect of slit width on the band shape of solid sodium sulfate (Na_2SO_4) using the 500 G/mm grating at 532 nm. The band shapes are very unresolved at the slit width of 300 µm.

Figure **16** shows an estimate of the spectral resolution in respect to the slit width of the spectrometer using a Pylon CCD. This information will be useful in the future when selecting an optimum slit size.

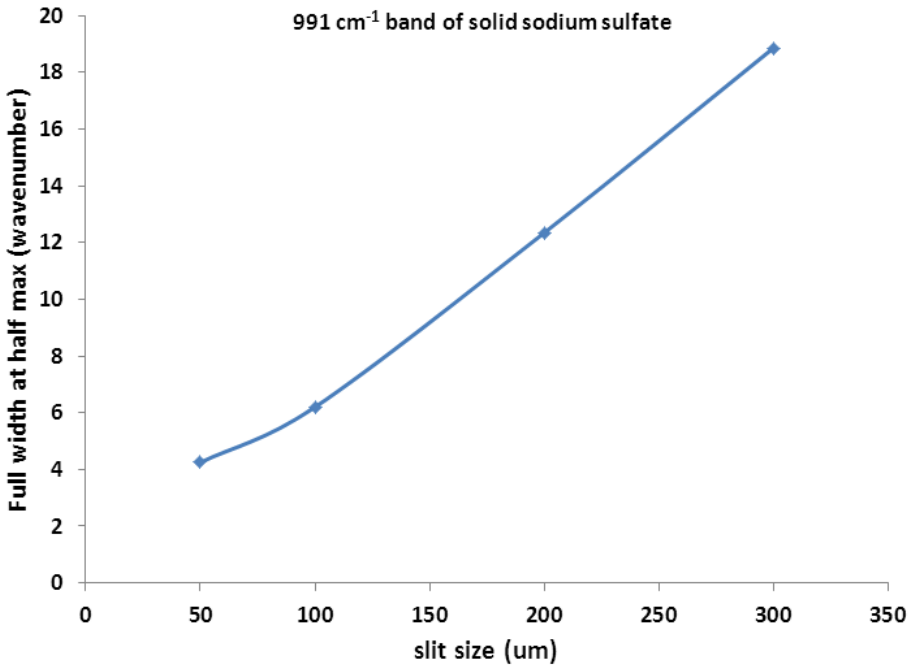

Figure 16. The effect of slit size on full width half max of 991 cm^{-1} band of solid Na_2SO_4

Beam size. In order to probe the Raman response only from the sample that is heated by the pump beam, the focused spot size of the probe beam must be smaller than the pump beam spot size. The initial measured probing beam size at the focus spot was ~400 μm and the heating beam size was ~200 μm. Clearly, the probing beam size needs to be smaller. The diffraction spot size using a spherical lens is determined by the following equation: $spot\ size = \frac{4M^2\lambda f}{\pi d} + \frac{nd^3}{f^2}$.[75] The first term is the diffraction component and the second term is the spherical aberration component from spherical lenses. In the first term, the spot size is proportional to M^2 which is the laser beam quality parameter, the laser wavelength (λ), and the focal length of the focus lens (f). The spot size is inversely proportional to the incident beam size (d).

We shaped the beam profile with an aperture to increase M^2 value and expanded the incident beam diameter using a beam expander (Thorlabs). The resulting focused beam diameter decreased to ~135 μm, which is smaller than the Pump beam diameter (Figure 17).

(a)

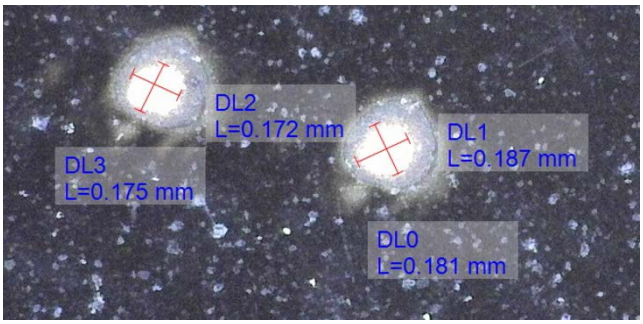

(b)

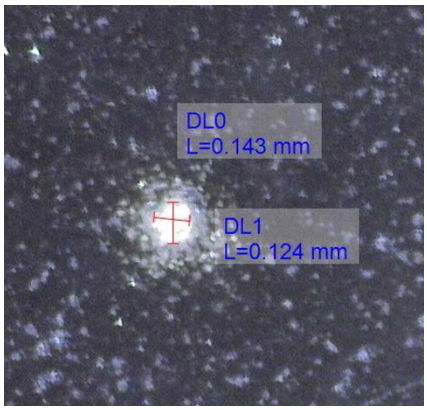

Figure 17. Images of burn papers showing the beam profiles of (a) pump beam and (b) probe beam at the sample position, taken from a microscope camera.

Flow cell. With the use of the pulse lasers, it is essential to replace each illuminated volume before the arrival of the next pulse. Therefore, a flow stream is often used for the sample. One of the most critical challenges in working with visible temperature jump is that the water absorbs very strongly at 1.9 μm region, water has an absorption coefficient of 40 cm^{-1} at 1.9 μm. As a result, the surface of the water stream will have the highest temperature change with the T-jump magnitude decreasing as the pump beam is absorbed by the sample (Figure 18a). However, the probe beam at 532 nm transmits through water. Due to the absorbance difference between these two wavelengths of light, the probe beam probes a distribution of temperature. A thin stream should be used in order to probe Raman scattering from the area of sample where there is a temperature change (Figure 18b).

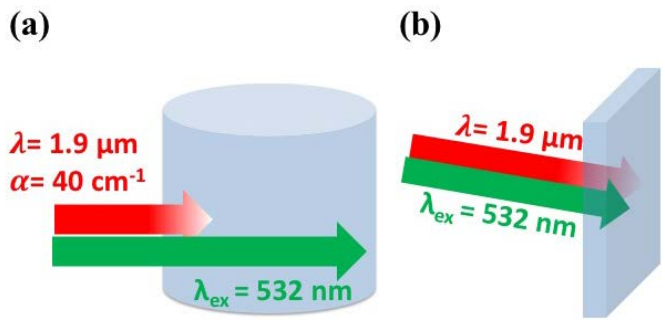

Figure 18. The absorption of the two laser beams in (a) a thick water stream (b) a thin water stream

A wire guided stream is used to achieve a ~100 μm thick free stream. As seen in Figure 19a, a stainless-steel wire (d=225 μm) was bent into an oval shape. The ends of the wire were fit into the nozzle of the flow cell. After the sample leaves the nozzle, it will run along the wires and form a thin sheet of sample stream. The thickness of the wire guided stream is approximately ~96 μm thin (Figure 19a), measured via absorbance of the pump beam (1.9 μm).

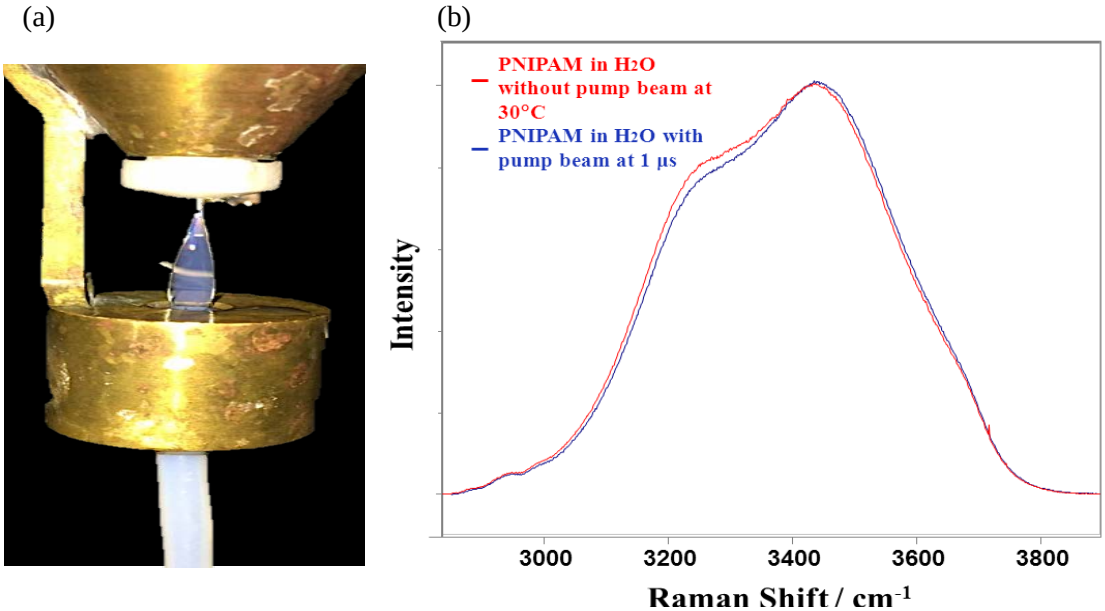

Figure 19. (a) Image of the wire guided PNIPAM stream (b) Visible Raman spectra (532-nm excitation) of PNIPAM in water (~1 wt%) without T-jump and with T-jump, integration time of 30 minutes per spectrum. The decrease in intensity in the water OH stretching region

A 20-degree T-jump experiment of PNIPAM was successfully done using the wire guided stream (Figure 19b). Unfortunately, at this concentration the CH stretching bands can

hardly be defined. This flow cell approach is ultimately limited by the concentration of PNIPAM to get enough signal of CH stretching bands. Because this is unlike the study of the amide group, we are no longer using Resonance Raman.

Cuvette. Flow cell limits the concentration of PNIPAM for the temperature jump study because a high concentration of PNIPAM sample tends to clog both flow cell and the pump. Therefore, a 100 μm flow cuvette was later used to introduce a more concentrated PNIPAM sample. To ensure we replace each illuminated volume before the arrival of the next pulse, peristaltic pump is incorporated to avoid this problem (Figure 20). This approach improved S/N for the Raman temperature jump spectra, allowing us to resolve the small shift in CH_3 anti-symmetric stretching band.

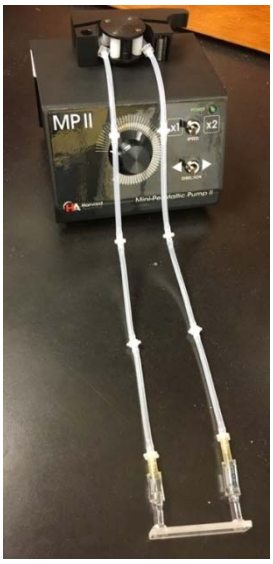

Figure 20. Concentrated sample set up for temperature jump experiment. A peristaltic pump is incorporated with a very short path length cuvette (0.1 mm).

5.0 EXAMINE THE KINETIC OF VPT USING TIME RESOLVED NORMAL RAMAN SPECTROSCOPY

Most phase transition studies of PNIPAM are studied in their equilibrium states. However, kinetics measurements are the key experimental tool to understanding the mechanism of PNIPAM VPT in sequence and time scale. And the kinetics of PNIPAM's hydrophobic collapse have not been studied much.[15, 74, 76-79]

In the case of VPT of PNIPAM, Ahmed *et al.*,[36] Reese *et al.*,[80] and Wang *et al.*[74] utilized T-jump method to understand the kinetics of VPT of PNIPAM. Wang *et al.* did a T-jump kinetic turbidity study on ~400 nm diameter PNIPAM hydrogel, which showed a single-exponential collapse with an apparent time constant of ~390 ns. Reese *et al.* on the other hand used T-jump absorption measurement and observed a multi-exponential collapse of ~350 nm nanogel. The whole collapse occurs with $\tau < 1$ μs and they showed an apparent mono-exponential collapse with τ ~120 ns for individual nanogel. They claimed the multi-exponential shrinking may result from differences in composition of the interior versus the periphery of these nanogel particles.[80] We hypothesized the VPT of PNIPAM occurs in three steps. Firstly, the dehydration of isopropyl groups, followed by a structural rearrangement of the monomers. Secondly, the dehydration of Amide groups. Finally, the dehydration and aggregation of the polymer main chains.

Ahmed *et al.* used time resolved UV Resonance Raman Spectroscopy and found the dehydration process of –C=O group in PNIPAM hydrogel has a mono-exponential collapse and occur within 360 ns and the dehydration of the amide group happens within ~1 μs.[36] To this day, little work has been done to look at the kinetics of dehydration of the hydrophobic groups of PNIPAM due to the many challenges presented studying the CH stretching bands in an extremely

short timescale, which is discussed in chapter 4. The timescale of isopropyl group's dehydration relative to the dehydration of hydrophilic groups will clarify the question of which group initiates the VPT of PNIPAM.

5.1 EXPERIMENTAL METHODS

Sample preparation. PNIPAM sample is prepared using the method described in Chapter 3 by Weissman *et al.*[61]. PNIPAM was concentrated by centrifuging the purified suspension at 17,000 rcf at 34°C for 70 minutes. The supernatant was removed and the final concentration was ~4 wt%. As illustrated in Figure 21, the PNIPAM sample is drawn using the mini peristaltic pump (Harvard apparatus) and fed into a 100 μm path length flow cuvette with a calculated velocity of 57.2 mm/s. The sample temperature was controlled by the water bath that was heated and monitored by an isotemp digital stirring hotplate (Fisher Scientific).

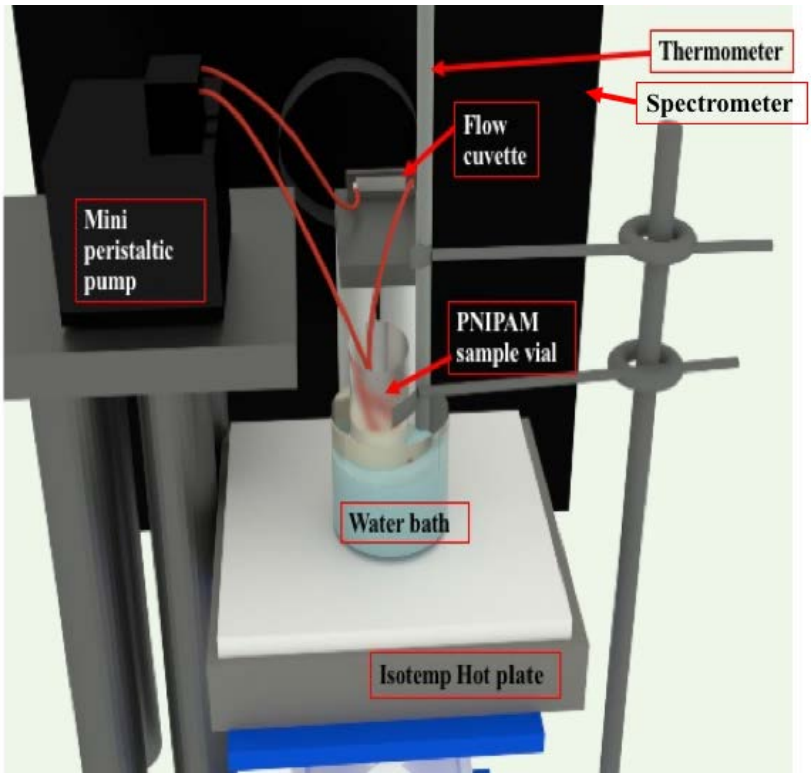

Figure 21. Sample set up of the normal Raman temperature jump experiment

Instrumentation. A T-jump result was obtained through the pump-probe set up that has been described in detail in Chapter 4. Briefly, the probe beam was a Coherent Infinity Nd:YAG laser produced 532-nm (second harmonic) 3-ns pulses at 100 Hz. The pump beam was obtained by using a 1 m Raman shifter (Light Age Inc., 1000 psi H_2) Raman shifted the 1064 nm fundamental wavelength to the first H_2 Stokes harmonic at 1.9 μm. This 1.9 μm excitation beam is strongly absorbed by water, where water has an absorption coefficient of 40 cm^{-1}.

Data Analysis. The degree of T-jump was determined using the method described by Lednev *et al.*.[44] The T-jump Raman spectra were normalized to the isosbestic point of liquid water OH stretching band at ~3425 cm^{-1}.[81] And the difference spectra is the result of a subtraction between PNIPAM with IR beam and PNIPAM without IR beam. Furthermore, the difference bands were fitted with a mixed of Gaussian and Lorentzian profile using the software GRAMS suite. The kinetic plot and time constant are obtained using the software Prism 7.

5.2 RESULTS AND DISCUSSION

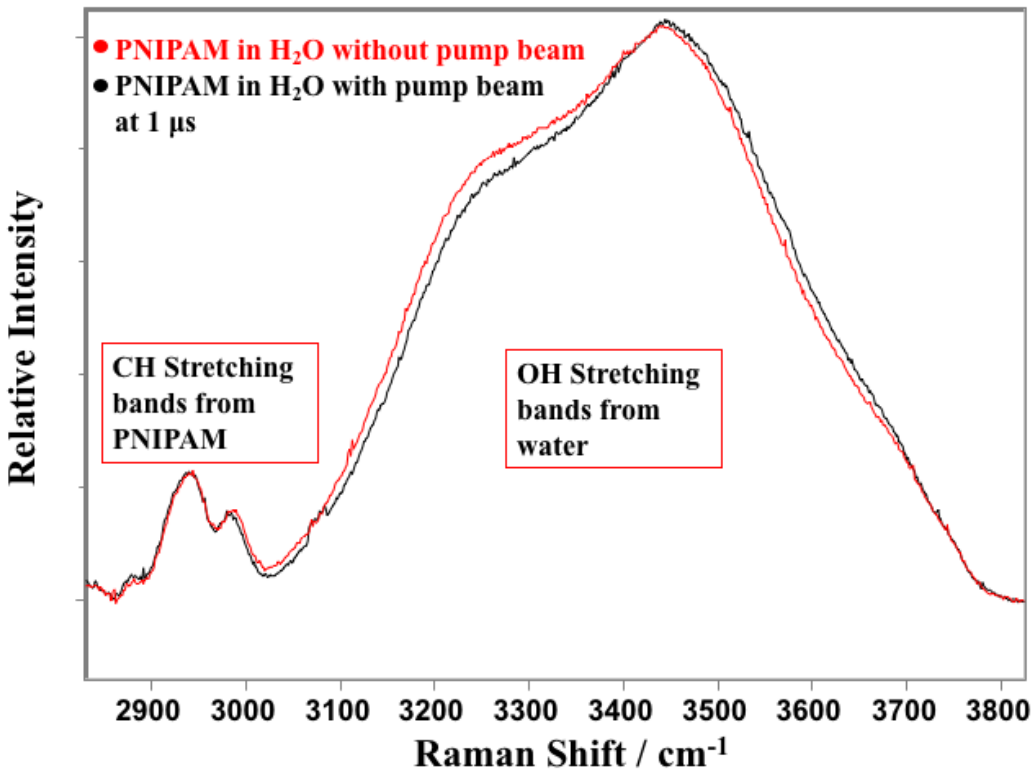

Figure 22. 532 nm- excited Raman spectra of PNIPAM in H_2O without temperature jump (red) and with temperature jump (black). The decrease in intensity in the water spectrum in the region 3000 – 3425 cm^{-1} indicates the temperature increase.

In order to determine the VPT reaction coordinate, we studied the dehydration kinetics of the isopropyl groups with time delays of 10, 50, 100, 150, 200, 500, 750, and 1000 ns, and monitored the frequency shift in the CH_3 anti-symmetric stretching, as shown in Figure 13, to be a marker for the hydration around the isopropyl groups. As seen in Figure 22, the PNIPAM spectrum with the pump beam (i.e. heating beam) indicates a 13.5 degree increase in temperature judging by the changes in OH stretching bands. As expected, we observe a small frequency shift in CH_3 anti-symmetric stretching band of PNIPAM upon crossing the LCST at 32°C. The 1 µs time delay is

shown because our previous studies found the hydrophobic collapse is completed by this time delay.[36]

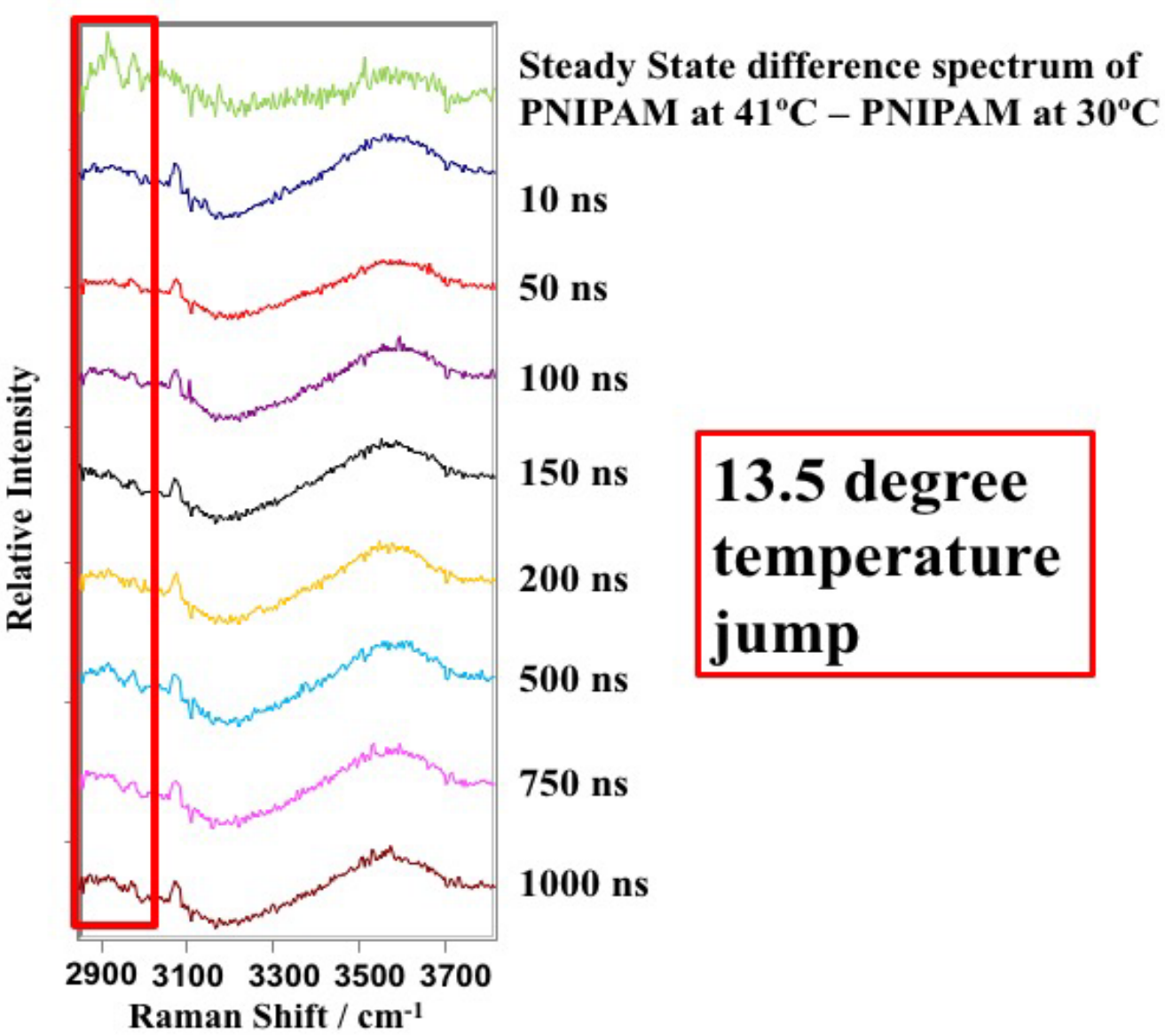

Figure 23. The difference spectra of PNIPAM before and after the VPT. The first spectrum is the steady state difference spectrum collected under the same experimental conditions. 13.5-degree T-jump difference spectra at different delay times are shown below the steady state spectrum in ascending order.

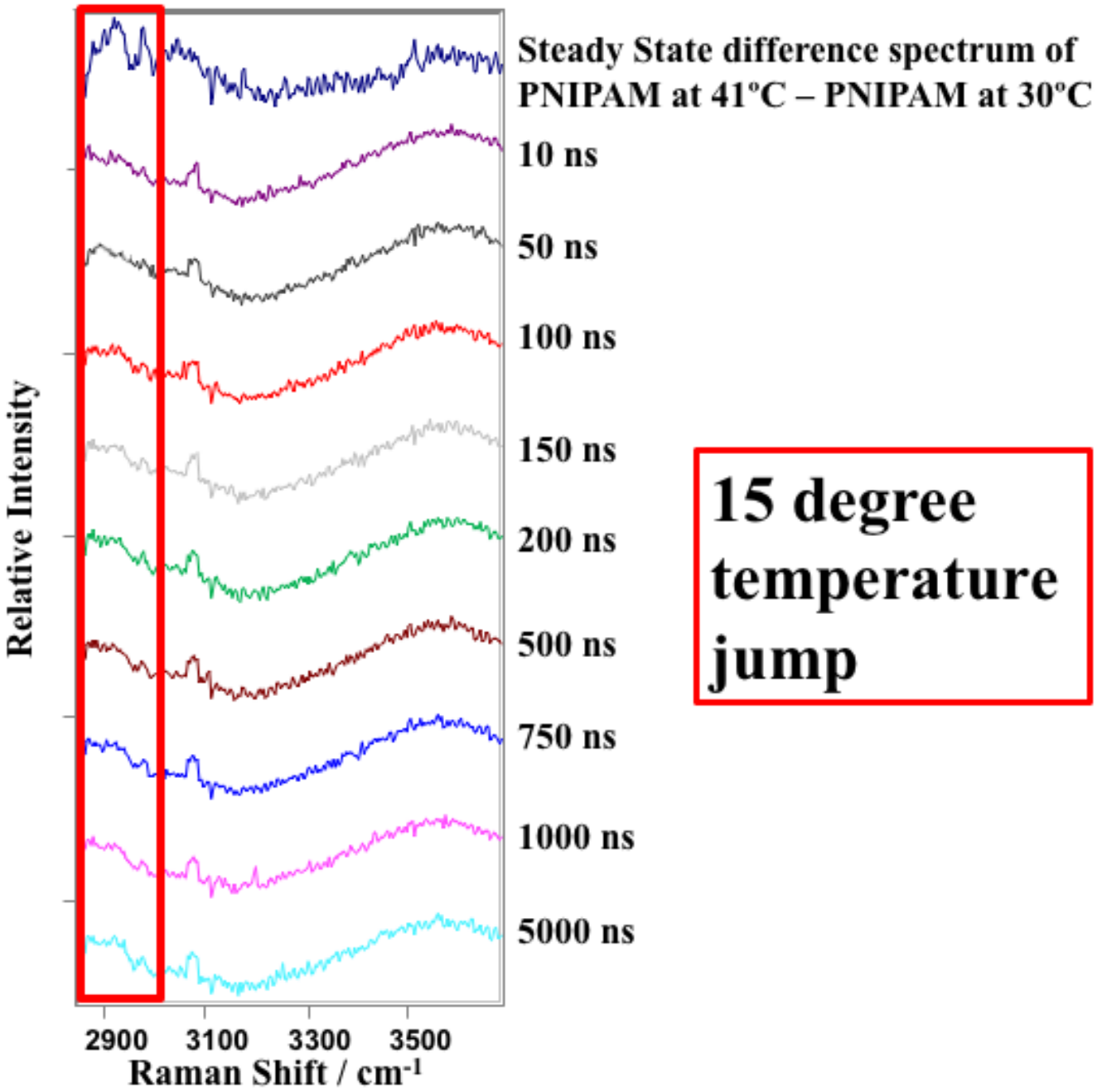

Figure 24. The difference spectra of PNIPAM below LCST and above LCST. The first spectrum is the steady state difference spectrum. 15-degree T-jump difference spectra at different delay times are shown below the steady state spectrum in ascending order.

Figure 23 and Figure 24 show two different T-jump experiments completed with a 13 and 15 temperature jumps at different time delays. Steady state difference spectrum of PNIPAM at

30ºC and 41ºC at the top of each figure show two peaks at ~2920 cm^{-1} and at ~2976 cm^{-1}. This difference arises from the frequency shift of CH_3 anti-symmetric stretching band. As discussed in Chapter 4, the PNIPAM sample is heated evenly during the steady state experiment. On the other hand, due to the absorbance difference between the pump and probe beams, temperature jump experiments have an exponential decrease of heat gradient as the probe beam penetrate deeper into the stream. Because of this, the T-jump spectra resulted in an average of the most heated to the least heated PNIPAM sample. Therefore, we do not expect the T-jump difference spectra to be as prominent as that of steady state difference spectra.

From the T-jump spectra collected in Figure 23 and Figure 24, we can study the dehydration kinetics of the hydrophobic CH groups. The CH_3 anti-symmetric stretching band starting to occur at 10 ns, otherwise, very little has happened at this delay time in the CH stretching region. The kinetics change in the CH_3 anti-symmetric stretching band can be modeled as a single exponential process which yields a time constant of 69 ± 8 (Figure 25). The steady state difference spectrum also shows a broad trough at ~2920 cm^{-1}. As Figure 23 and Figure 24 shown, this difference arises shortly after the frequency shift of CH_3 anti-symmetric stretching band. This difference can be attributed from the dehydration and aggregation of the polymer chains (CH-CH_2-). We have assigned CH_2 anti-symmetric stretching at ~2920 cm^{-1} (see Figure 28 in Appendix A for more information). The CH_2 anti-symmetric stretching can be seen starting ~100 ns, and these difference peaks grow with an increase of delay time. This can also be modeled as a single exponential process which yields a time constant 104 ± 44 (Figure 26).

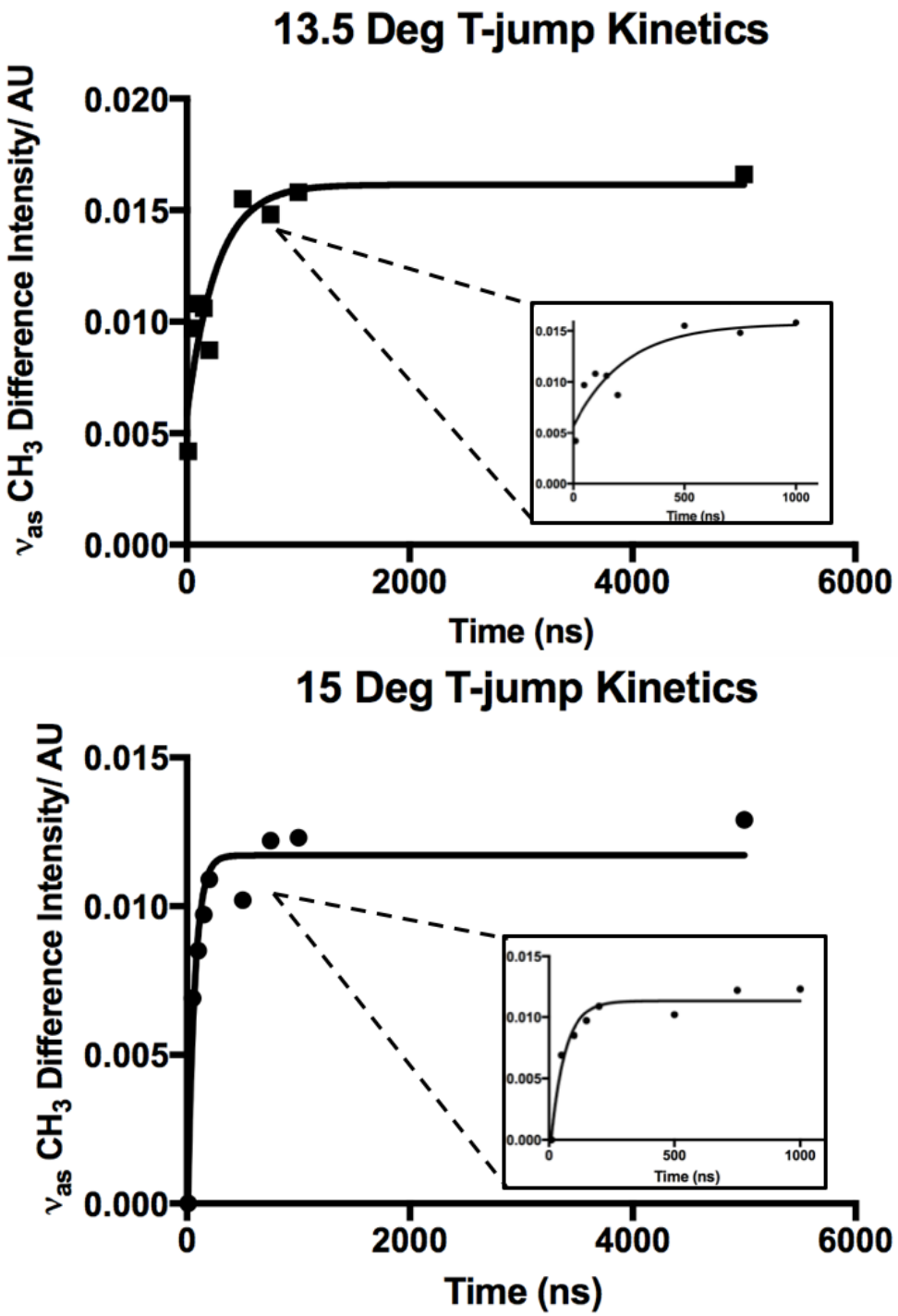

Figure 25. (Top) The dehydration kinetics plot of the CH_3 anti-symmetric stretching band from the 13.5-degree T-jump experiment, which yields a time constant of 72. (Bottom) The dehydration kinetics plot of the CH_3 anti-symmetric stretching band from the 15-degree T-jump experiment, which yields a time constant of 63.

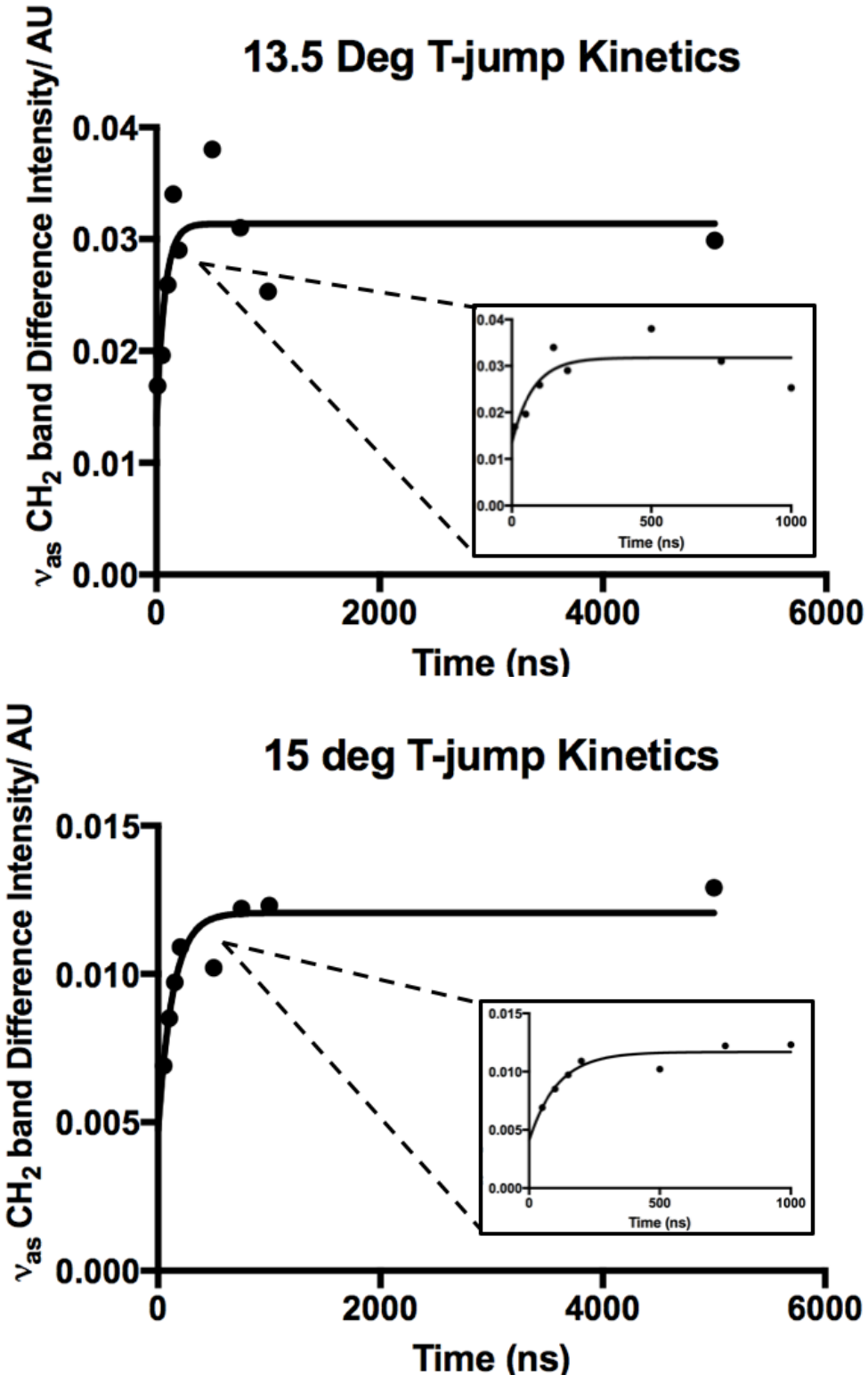

Figure 26. (Top) The dehydration kinetics plot of the CH_2 antisymmetric stretching band from the 13.5-degree T-jump experiment, which yields a time constant of 73. (Bottom) The dehydration kinetics plot of the CH_2 antisymmetric stretching band from the 15-degree T-jump experiment, which yields a time constant of 135.

Our result is closest to the FT-IR and 2D-COS work done by Sun *et al.*,[12] who studied PNIPAM in D_2O. They found that hydrophobic groups almost immediately dehydrate as soon as the temperature elevates. Hydrophilic groups, however, undergo transition until the temperature is passed the LCST. The CH_3 groups start the LCST phase separation with a two-step dehydration, the main chains follow by diffusion and aggregation, amide groups then give up their hydrogen bonds with water, and finally the inter-amide hydrogen bonds stabilize the globular state of the polymer chains. Our Raman kinetics studies show a similar order of reaction that was proposed by Sun *et al*. However, our studies did not show a two-step dehydration event for the isopropyl groups. We believe it is purely a single exponential process (Figure 25). This difference can be attributed to the solvent used in the studies (D_2O versus H_2O). Alternatively, the two-step dehydration events of isopropyl groups might occur faster than the nanosecond timescales studied here. Further computational studies need to be done to confirm the results. Our result depicted that the molecular mechanism of the VPT for PNIPAM is the following: dehydration of the isopropyl groups occurs first at ~68 ns, shortly after there is some dehydration of the polymer chains at ~104 ns. Finally, the dehydration of the amide groups occurs at ~360 ns.[36]

5.3 CONCLUSION

PNIPAM has been selected as a model system to study the polymer hydrophobic collapse due to its large response to stimuli and the fast response time. In our study, we utilized DLS, UV Resonance Raman, and time resolved normal Raman spectroscopy to investigate the molecular mechanism of the PNIPAM volume phase transition. Our results clearly show that the hydrophobic groups initiate the VPT. This clarifies the controversial topic scientists have about VPT of

PNIPAM. In Table 3, we summarized the molecular mechanism of PNIPAM VPT. We proposed the molecular mechanism of VPT as dehydration of the isopropyl groups → dehydration and aggregation of the methylene groups from the polymer chains → dehydration of the amide groups. Our spectroscopic data monitor the frequency shift of selected bands, which is due to the hydration and dehydration of the PNIPAM. Therefore, solvent interaction plays a huge role in hydrophobic collapse. Future work that can benefit further understanding of VPT in the molecular level will be investigating the water OH stretching bands and low frequency water OH bending bands. This will give us useful insights on the micro dynamics of hydrating water and bulk water undergoes VPT.

Table 3. Time ordering of PNIPAM VPT

Time Constant (ns)	Spectral Changes	Molecular Dynamics
69 ± 8	CH_3 anti-symmetric stretching band downshifts to lower frequency (~2976 cm^{-1})	Isopropyl groups hydrophobic collapse; CH_3 dehydration
104 ± 44	CH_2 anti-symmetric stretching band downshifts to lower frequency (~2920 cm^{-1})	(-CH-CH_2) dehydration and aggregation
360 ± 85 [36]	AmI band frequency upshifts; decreased H_2O [36]	C=O-H-bonded water cluster collapse; C=O dehydration [36]

APPENDIX A

BAND ASSIGNMENT OF C-H STRETCHING BANDS OF PNIPAM

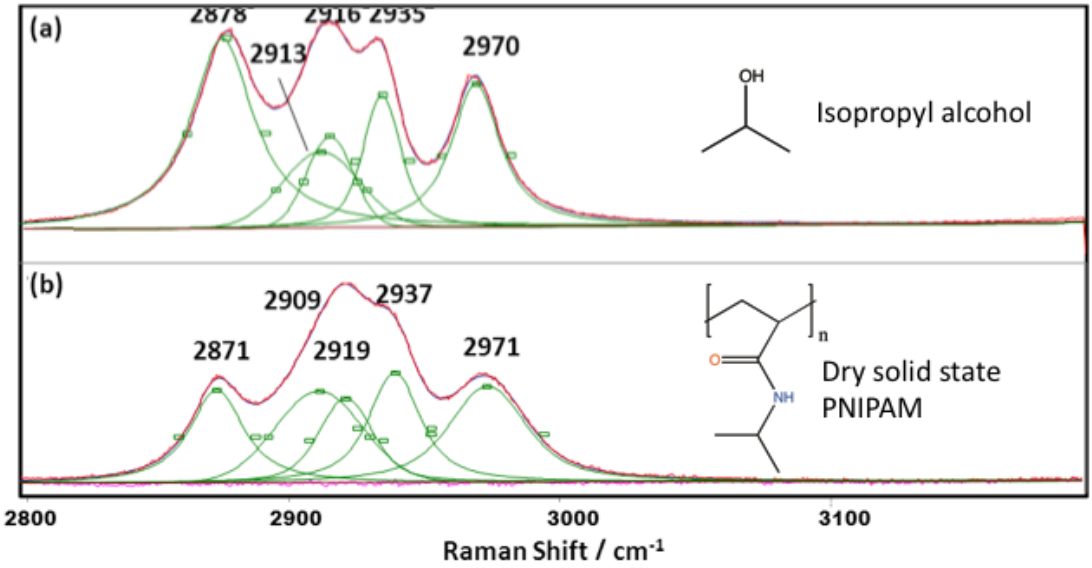

Figure 27. 633-nm excited Raman spectrum C-H stretching region of (a) liquid isopropyl alcohol, (b) solid state PNIPAM. All the Raman bands are fitted with a Voigt profile as shown.

Figure 27 shows the deconvoluted bands of isopropyl alcohol and solid state PNIPAM. They show similar band shapes and vibration since both of them contain isopropyl groups. The only significant difference is the first C-H stretching band around ~2870 cm^{-1}. This frequency difference might be due to the presence of additional methylene group in PNIPAM backbone since the symmetric stretching of methylene is at this region (Figure 27).

The spectral assignment for isopropyl alcohol in the C-H stretching region has been controversial. Furthermore, the assignment for either isopropyl alcohol or PNIPAM was often ambiguous or failed to recognize that the Fermi resonance mode generally exists in the C-H

stretching region. A recent study done by Liu *et al*. clarified the CH stretching bands assignment of isopropyl alcohol.[66]

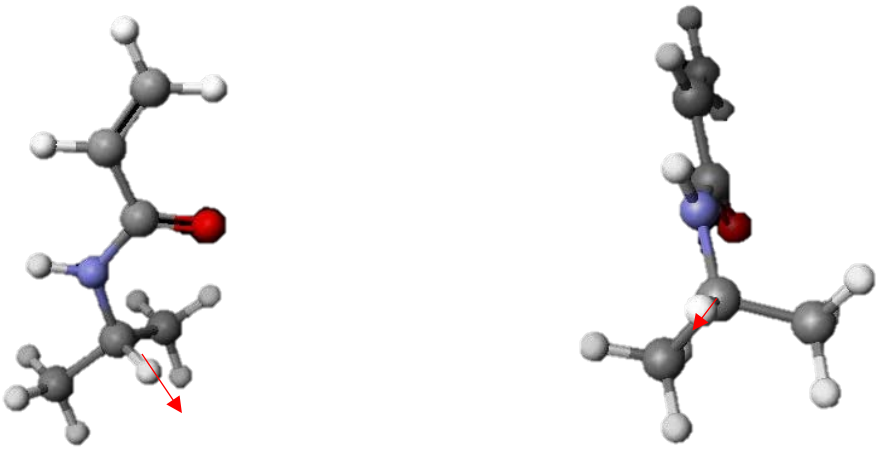

Figure 28. Geometry structure of NIPAM in the two conformers. The red arrow shows the stretching motion of CH group for (left) the Gauche conformer and (right) the Trans conformer

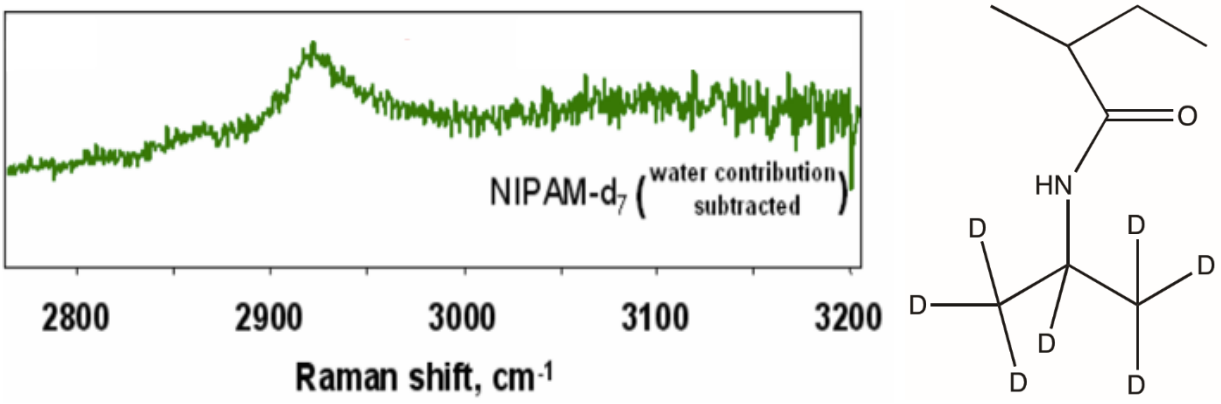

Figure 29. 488-nm excited NIPAM-d_7 spectrum at the CH stretching region after water subtraction and the structure of the NIPAM-d_7.

The first peak in PNIPAM at ~2871cm^{-1} shows a slight downshift in frequency compareto isopropyl alcohol. The frequency of methylene group is known to be ~2880 cm^{-1} for symmetric stretching,[53] which is overlapped with the stretching band of the gauche conformer of the -CH group. Further evidence is found in the 488-nm excited Raman spectrum of NIPAM-d_7 previously collected by Pimenov *et al*. (Figure 29). This is to ensure the CH stretching vibration is only from the methylene back bone. They observed two CH stretching bands around ~2860 cm^{-1} and ~2920

cm^{-1}. According to Liu *et al.*, there also might be some Fermi resonance coupling with the overtone of CH bending band, which then enhanced by the CH-str-gauche and CH_2 symmetric stretching motions. The second band at ~2909 cm^{-1} is assigned to the Fermi resonance of the CH_3 deformation overtone band that has a fundamental band located around 1455cm^{-1} (Figure 6). The third band at ~2919 cm^{-1} is assigned to an overlapping of the Fermi resonance of the overtone/ combination band of CH_3 bending and the asymmetric stretching of the methylene band. A very weak contribution of trans conformer of CH symmetric stretch vibration (Figure 28) is also overlapping with this band. The band at 2937 cm^{-1} corresponds to the CH_3 symmetric stretching vibration while the band at 2971 cm^{-1} is from the CH_3 asymmetric stretching. Normal mode studies need to be done to verify the CH stretching bands assignment for PNIPAM. The assignment of C-H stretching bands allows us to explain the frequency shift contributions in our T-jump spectra and toward determining the reaction coordinate of PNIPAM VPT.

Table 4. Spectral assignment of 633-nm excited Raman spectrum of isopropyl alcohol and solid state PNIPAM

	Raman frequency/ cm^{-1}	Spectral assignment	Previous assignment[84]
Isopropyl alcohol	2878	CH_3-FR and CH-str-gauche	2879
	2913	CH_3-FR	2911
	2916	CH_3-FR and CH-str-trans	2920
	2935	CH_3-SS	2938
	2970	CH_3-AS	2973
Dehydrated solid state PNIPAM	2871	CH_3-FR and CH-str-gauche and CH_2 symmetric str	
	2909	CH_3-FR	
	2919	CH_3-FR and CH-str-trans and CH_2 asymmetric str	
	2937	CH_3-SS	
	2971	CH_3-AS	

BIBLIOGRAPHY

1. Lumry, R.; Biltonen, R.; Brandts, J. F., Validity of the "two-state" hypothesis for conformational transitions of proteins. *Biopolymers* **1966,** *4* (8), 917-944.
2. Privalov, P. L., Stability of proteins small globular proteins. *Advances in protein chemistry* **1979,** *33*, 167-241.
3. Winnik, F. M.; Ottaviani, M. F.; Bossman, S. H.; Pan, W.; Garcia-Garibay, M.; Turro, N. J., Phase separation of poly(N-isopropylacrylamide) in water: a spectroscopic study of a polymer tagged with a fluorescent dye and a spin label. *The Journal of Physical Chemistry* **1993,** *97* (49), 12998-13005.
4. Ottaviani, M. F.; Winnik, F. M.; Bossmann, S. H.; Turro, N. J., Phase Separation of Poly(N-isopropylacrylamide) in Mixtures of Water and Methanol: A Spectroscopic Study of the Phase-Transition Process with a Polymer Tagged with a Fluorescent Dye and a Spin Label. *Helvetica Chimica Acta* **2001,** *84* (9), 2476-2492.
5. Chee, C. K.; Rimmer, S.; Soutar, I.; Swanson, L., Fluorescence investigations of the thermally induced conformational transition of poly(N-isopropylacrylamide). *Polymer* **2001,** *42* (12), 5079-5087.
6. Tam, K. C.; Wu, X. Y.; Pelton, R. H., Viscometry—a useful tool for studying conformational changes of poly(N-isopropylacrylamide) in solutions. *Polymer* **1992,** *33* (2), 436-438.
7. Burba, C. M.; Carter, S. M.; Meyer, K. J.; Rice, C. V., Salt Effects on Poly(N-isopropylacrylamide) Phase Transition Thermodynamics from NMR Spectroscopy. *The Journal of Physical Chemistry B* **2008,** *112* (34), 10399-10404.
8. Dybal, J.; Trchová, M.; Schmidt, P., The role of water in structural changes of poly (N-isopropylacrylamide) and poly (N-isopropylmethacrylamide) studied by FTIR, Raman spectroscopy and quantum chemical calculations. *Vibrational Spectroscopy* **2009,** *51* (1), 44-51.
9. Katsumoto, Y.; Tanaka, T.; Sato, H.; Ozaki, Y., Conformational Change of Poly(N-isopropylacrylamide) during the Coil−Globule Transition Investigated by Attenuated Total Reflection/Infrared Spectroscopy and Density Functional Theory Calculation. *The Journal of Physical Chemistry A* **2002,** *106* (14), 3429-3435.
10. Lai, H.; Wu, P., A infrared spectroscopic study on the mechanism of temperature-induced phase transition of concentrated aqueous solutions of poly(N-isopropylacrylamide) and N-isopropylpropionamide. *Polymer* **2010,** *51* (6), 1404-1412.
11. Ramon, O.; Kesselman, E.; Berkovici, R.; Cohen, Y.; Paz, Y., Attenuated total reflectance/Fourier transform infrared studies on the phase-separation process of aqueous solutions of poly(N-isopropylacrylamide). *J. Polym. Sci. B: Polym. Phys.* **2001,** *39* (14), 1665-1677.
12. Sun, B.; Lin, Y.; Wu, P.; Siesler, H. W., A FTIR and 2D-IR Spectroscopic Study on the Microdynamics Phase Separation Mechanism of the Poly(N-isopropylacrylamide) Aqueous Solution. *Macromolecules* **2008,** *41* (4), 1512-1520.
13. Sun, S.; Hu, J.; Tang, H.; Wu, P., Chain Collapse and Revival Thermodynamics of Poly(N-isopropylacrylamide) Hydrogel. *The Journal of Physical Chemistry B* **2010,** *114* (30), 9761-9770.

14. Tong, Y.; Kampfrath, T.; Campen, R. K., Experimentally probing the libration of interfacial water: the rotational potential of water is stiffer at the air/water interface than in bulk liquid. *Physical Chemistry Chemical Physics* **2016,** *18* (27), 18424-18430.
15. Deshmukh, S. A.; Kamath, G.; Suthar, K. J.; Mancini, D. C.; Sankaranarayanan, S. K. R. S., Non-equilibrium effects evidenced by vibrational spectra during the coil-to-globule transition in poly(N-isopropylacrylamide) subjected to an ultrafast heating-cooling cycle. *Soft Matter* **2014,** *10* (10), 1462-1480.
16. Pelton, R., Temperature-sensitive aqueous microgels. *Advances in Colloid and Interface Science* **2000,** *85* (1), 1-33.
17. Kang Derwent, J. J.; Mieler, W. F., Thermoresponsive Hydrogels as a New Ocular Drug Delivery Platform to The Posterior Segment of the Eye. *Transactions of the American Ophthalmological Society* **2008,** *106*, 206-214.
18. Palomino, K.; Suarez-Meraz, K. A.; Serrano-Medina, A.; Olivas, A.; Samano, E. C.; Cornejo-Bravo, J. M., Microstructured poly(N-isopropylacrylamide) hydrogels with fast temperature response for pulsatile drug delivery. *Journal of Polymer Research* **2015,** *22* (10), 1-9.
19. Islam, M. R.; Li, X.; Smyth, K.; Serpe, M. J., Polymer-Based Muscle Expansion and Contraction. *Angewandte Chemie International Edition* **2013,** *52* (39), 10330-10333.
20. Hendrickson, G. R.; Andrew Lyon, L., Bioresponsive hydrogels for sensing applications. *Soft Matter* **2009,** *5* (1), 29-35.
21. Oktar, O.; Caglar, P.; Seitz, W. R., Chemical modulation of thermosensitive poly(N-isopropylacrylamide) microsphere swelling: a new strategy for chemical sensing. *Sensors and Actuators B: Chemical* **2005,** *104* (2), 179-185.
22. Holtz, J. H.; Asher, S. A., Polymerized colloidal crystal hydrogel films as intelligent chemical sensing materials. *Nature* **1997,** *389* (6653), 829-832.
23. Mutlu, S.; Yu, C.; Svec, F.; Mastrangelo, C. H.; Fréchet, J. M. J.; Gianchandani, Y. B. In *A thermally responsive polymer microvalve without mechanical parts photo-patterned in a parylene channel*, TRANSDUCERS 2003 - 12th International Conference on Solid-State Sensors, Actuators and Microsystems, Digest of Technical Papers, 2003; pp 802-805.
24. Richter, A.; Howitz, S.; Kuckling, D.; Arndt, K.-F., Influence of volume phase transition phenomena on the behavior of hydrogel-based valves. *Sensors and Actuators B: Chemical* **2004,** *99* (2–3), 451-458.
25. Sorrell, C. D.; Carter, M. C. D.; Serpe, M. J., Color Tunable Poly (N-Isopropylacrylamide)-co-Acrylic Acid Microgel–Au Hybrid Assemblies. *Advanced Functional Materials* **2011,** *21* (3), 425-433.
26. Sorrell, C. D.; Serpe, M. J., Reflection Order Selectivity of Color-Tunable Poly(N-isopropylacrylamide) Microgel Based Etalons. *Advanced Materials* **2011,** *23* (35), 4088-4092.
27. Bischofberger, I.; Calzolari, D. C. E.; De Los Rios, P.; Jelezarov, I.; Trappe, V., Hydrophobic hydration of poly-N-isopropyl acrylamide: a matter of the mean energetic state of water. *Scientific Reports* **2014,** *4*, 4377.
28. Flory, P. J., *Principles of Polymer Chemistry*. Cornell University Press: 1953.
29. Hirotsu, S.; Hirokawa, Y.; Tanaka, T., Volume-phase transitions of ionized N-isopropylacrylamide gels. *The Journal of Chemical Physics* **1987,** *87* (2), 1392-1395.
30. Schmaljohann, D., Thermo-and pH-responsive polymers in drug delivery. *Advanced drug delivery reviews* **2006,** *58* (15), 1655-1670.
31. Galamba, N., Water's Structure around Hydrophobic Solutes and the Iceberg Model. *The Journal of Physical Chemistry B* **2013,** *117* (7), 2153-2159.

32. Kauzmann, W., Some factors in the interpretation of protein denaturation. *Advances in protein chemistry* **1959,** *14*, 1-63.
33. Cai, S.; Suo, Z., Mechanics and chemical thermodynamics of phase transition in temperature-sensitive hydrogels. *Journal of the Mechanics and Physics of Solids* **2011,** *59* (11), 2259-2278.
34. Terada, T.; Inaba, T.; Kitano, H.; Maeda, Y.; Tsukida, N., Raman spectroscopic study on water in aqueous solutions of temperature-responsive polymers: Poly(N-isopropylacrylamide) and poly[N-(3-ethoxypropyl)acrylamide]. *Macromolecular Chemistry and Physics* **1994,** *195* (9), 3261-3270.
35. Suzuki, Y.; Suzuki, N.; Takasu, Y.; Nishio, I., A study on the structure of water in an aqueous solution by the solvent effect on a volume phase transition of N-isopropylacrylamide gel and low-frequency Raman spectroscopy. *The Journal of chemical physics* **1997,** *107* (15), 5890-5897.
36. Ahmed, Z.; Gooding, E. A.; Pimenov, K. V.; Wang, L.; Asher, S. A., UV Resonance Raman Determination of Molecular Mechanism of Poly(N-isopropylacrylamide) Volume Phase Transition. *The Journal of Physical Chemistry B* **2009,** *113* (13), 4248-4256.
37. Haken, H.; Wolf, H. C., *Molecular Physics and Elements of Quantum Chemistry: Introduction to Experiments and Theory*. Springer: 2004.
38. Smith, E.; Dent, G., *Modern Raman Spectroscopy: a practical approach*. Wiley: 2005.
39. Bernath, P. F., *Spectra of Atoms and Molecules*. Oxford University Press: 2005.
40. Colthup, N. B.; Daly, L. H.; Wiberley, S. E., *Introduction to Infrared and Raman Spectroscopy*. Elsevier: 1990.
41. Glockler, G., The Raman Effect. *Reviews of Modern Physics* **1943,** *15* (2), 111-173.
42. Gordon, K. C.; Fraser-Miller, S. J., Raman Spectroscopy. In *Analytical Techniques in the Pharmaceutical Sciences*, Springer: 2016; pp 139-169.
43. Schrader, B., *Infrared and Raman Spectroscopy: Methods and Applications*. John Wiley & Sons: 2008.
44. Lednev, I. K.; Karnoup, A. S.; Sparrow, M. C.; Asher, S. A., α-Helix peptide folding and unfolding activation barriers: a nanosecond UV resonance Raman study. *Journal of the American Chemical Society* **1999,** *121* (35), 8074-8086.
45. Lednev, I. K.; Karnoup, A. S.; Sparrow, M. C.; Asher, S. A., Nanosecond UV resonance Raman examination of initial steps in α-helix secondary structure evolution. In *Spectroscopy of Biological Molecules: New Directions*, Springer: 1999; pp 11-12.
46. Pimenov, K. V. UV RAMAN INVESTIGATION OF PEPTIDEHYDRATION AND HYDROPHOBIC COLLAPSE. University of Pittsburgh, 2007.
47. Maeda, Y.; Higuchi, T.; Ikeda, I., Change in Hydration State during the Coil−Globule Transition of Aqueous Solutions of Poly(N-isopropylacrylamide) as Evidenced by FTIR Spectroscopy. *Langmuir* **2000,** *16* (19), 7503-7509.
48. Juurinen, I.; Galambosi, S.; Anghelescu-Hakala, A. G.; Koskelo, J.; Honkimäki, V.; Hämäläinen, K.; Huotari, S.; Hakala, M., Molecular-Level Changes of Aqueous Poly(N-isopropylacrylamide) in Phase Transition. *The Journal of Physical Chemistry B* **2014,** *118* (20), 5518-5523.
49. Deshmukh, S. A.; Sankaranarayanan, S. K.; Mancini, D. C., Vibrational spectra of proximal water in a thermo-sensitive polymer undergoing conformational transition across the lower critical solution temperature. *The journal of physical chemistry B* **2012,** *116* (18), 5501-5515.

50. Oh, S. Y.; Kim, H. J.; Bae, Y. C., Molecular thermodynamic analysis for phase transitions of linear and cross-linked poly(N-isopropylacrylamide) in water/2-propanol mixtures. *Polymer* **2013,** *54* (25), 6776-6784.
51. Speer, M. RAMAN SPECTROSCOPY AS A TECHNIQUE FOR STUDYING THE STRUCTURE AND MECHANISM OF THE VOLUME PHASE TRANSITION OF POLY (N--ISOPROPYLACRYLAMIDE. University of Pittsburgh, 2013.
52. Schmidt, P.; Dybal, J.; Trchová, M., Investigations of the hydrophobic and hydrophilic interactions in polymer–water systems by ATR FTIR and Raman spectroscopy. *Vibrational spectroscopy* **2006,** *42* (2), 278-283.
53. Snyder, R.; Hsu, S.; Krimm, S., Vibrational spectra in the C H stretching region and the structure of the polymethylene chain. *Spectrochimica Acta Part A: Molecular Spectroscopy* **1978,** *34* (4), 395-406.
54. Gu, Y.; Kar, T.; Scheiner, S., Fundamental Properties of the CH⊙⊙⊙ O Interaction: Is It a True Hydrogen Bond? *Journal of the American Chemical Society* **1999,** *121* (40), 9411-9422.
55. Hobza, P.; Havlas, Z., Blue-shifting hydrogen bonds. *Chemical reviews* **2000,** *100* (11), 4253-4264.
56. Qian, W.; Krimm, S., Vibrational Spectroscopy of Hydrogen Bonding: Origin of the Different Behavior of the CH⊙⊙⊙ O Hydrogen Bond. *The Journal of Physical Chemistry A* **2002,** *106* (28), 6628-6636.
57. Bykov, S. V.; Myshakina, N. S.; Asher, S. A., Dependence of glycine CH2 stretching frequencies on conformation, ionization state, and hydrogen bonding. *The Journal of Physical Chemistry B* **2008,** *112* (18), 5803-5812.
58. Deshmukh, S. A.; Sankaranarayanan, S. K. R. S.; Suthar, K.; Mancini, D. C., Role of Solvation Dynamics and Local Ordering of Water in Inducing Conformational Transitions in Poly(N-isopropylacrylamide) Oligomers through the LCST. *The Journal of Physical Chemistry B* **2012,** *116* (9), 2651-2663.
59. Ni, Y.; Gruenbaum, S. M.; Skinner, J. L., Slow hydrogen-bond switching dynamics at the water surface revealed by theoretical two-dimensional sum-frequency spectroscopy. *Proceedings of the National Academy of Sciences of the United States of America* **2013,** *110* (6), 1992-1998.
60. Tamai, Y.; Tanaka, H.; Nakanishi, K., Molecular Dynamics Study of Polymer−Water Interaction in Hydrogels. 1. Hydrogen-Bond Structure. *Macromolecules* **1996,** *29* (21), 6750-6760.
61. Weissman, J. M.; Sunkara, H. B.; Tse, A. S.; Asher, S. A. *Thermally Switchable Periodicities and Diffraction from Novel Mesoscopically Ordered Materials*; DTIC Document: 1996.
62. Bykov, S.; Lednev, I.; Ianoul, A.; Mikhonin, A.; Munro, C.; Asher, S. A., Steady-state and transient ultraviolet resonance Raman spectrometer for the 193–270 nm spectral region. *Appl. Spectrosc.* **2005,** *59* (12), 1541-1552.
63. Reider, G. A.; Traar, K. P.; Schmidt, A. J., Thin fluid jet stream of high optical quality. *Appl. Opt.* **1984,** *23* (17), 2856-2857.
64. Asher, S. A.; Ianoul, A.; Mix, G.; Boyden, M. N.; Karnoup, A.; Diem, M.; Schweitzer-Stenner, R., Dihedral ψ angle dependence of the amide III vibration: A uniquely sensitive UV resonance Raman secondary structural probe. *Journal of the American Chemical Society* **2001,** *123* (47), 11775-11781.
65. Mayne, L. C.; Hudson, B., Resonance Raman spectroscopy of N-methylacetamide: overtones and combinations of the carbon-nitrogen stretch (amide II') and effect of solvation on

the carbon-oxygen double-bond stretch (amide I) intensity. *The Journal of Physical Chemistry* **1991,** *95* (8), 2962-2967.
66. Yu, Y.; Wang, Y.; Hu, N.; Lin, K.; Zhou, X.; Liu, S., Overlapping spectral features and new assignment of 2-propanol in the C–H stretching region. *Journal of Raman Spectroscopy* **2014,** *45* (3), 259-265.
67. Hermansson, K., Blue-shifting hydrogen bonds. *The Journal of Physical Chemistry A* **2002,** *106* (18), 4695-4702.
68. Hobza, P.; Havlas, Z., Improper, blue-shifting hydrogen bond. *Theoretical Chemistry Accounts* **2002,** *108* (6), 325-334.
69. Keefe, C. D.; Gillis, E. A.; MacDonald, L., Improper hydrogen-bonding CH· Y interactions in binary methanol systems as studied by FTIR and Raman spectroscopy. *The Journal of Physical Chemistry A* **2009,** *113* (11), 2544-2550.
70. van der Veken, B. J.; Herrebout, W. A.; Szostak, R.; Shchepkin, D. N.; Havlas, Z.; Hobza, P., The nature of improper, blue-shifting hydrogen bonding verified experimentally. *Journal of the American Chemical Society* **2001,** *123* (49), 12290-12293.
71. Eigen, M., Immeasurably fast reactions. *Nobel Lecture* **1967,** *11*, 1963-1979.
72. Kubelka, J., Time-resolved methods in biophysics. 9. Laser temperature-jump methods for investigating biomolecular dynamics. *Photochemical & Photobiological Sciences* **2009,** *8* (4), 499-512.
73. Yamamoto, K.; Mizutani, Y.; Kitagawa, T., Construction of Novel Nanosecond Temperature Jump Apparatuses Applicable to Raman Measurements and Direct Observation of Transient Temperature. *Appl. Spectrosc.* **2000,** *54* (11), 1591-1604.
74. Wang, J.; Gan, D.; Lyon, L. A.; El-Sayed, M. A., Temperature-Jump Investigations of the Kinetics of Hydrogel Nanoparticle Volume Phase Transitions. *Journal of the American Chemical Society* **2001,** *123* (45), 11284-11289.
75. Bykov, S. V.; Sharma, B.; Asher, S. A., High-throughput, high-resolution Echelle deep-UV Raman spectrometer. *Appl. Spectrosc.* **2013,** *67* (8), 873-883.
76. Okajima, T.; Harada, I.; Nishio, K.; Hirotsu, S., Kinetics of volume phase transition in poly(N-isopropylacrylamide) gels. *The Journal of Chemical Physics* **2002,** *116* (20), 9068-9077.
77. Sato Matsuo, E.; Tanaka, T., Kinetics of discontinuous volume–phase transition of gels. *The Journal of Chemical Physics* **1988,** *89* (3), 1695-1703.
78. Shibayama, M.; Nagai, K., Shrinking Kinetics of Poly(N-isopropylacrylamide) Gels T-Jumped across Their Volume Phase Transition Temperatures. *Macromolecules* **1999,** *32* (22), 7461-7468.
79. Takahashi, K.; Takigawa, T.; Masuda, T., Swelling and deswelling kinetics of poly(N-isopropylacrylamide) gels. *The Journal of Chemical Physics* **2004,** *120* (6), 2972-2979.
80. Reese, C. E.; Mikhonin, A. V.; Kamenjicki, M.; Tikhonov, A.; Asher, S. A., Nanogel nanosecond photonic crystal optical switching. *Journal of the American Chemical Society* **2004,** *126* (5), 1493-1496.
81. Walrafen, G. E.; Hokmabadi, M. S.; Yang, W. H., Raman isosbestic points from liquid water. *The Journal of Chemical Physics* **1986,** *85* (12), 6964-6969.